Journal of Medicinal Chemistry

Drug Annotation

Discovery of a First-in-Class Receptor Interacting Protein 1 (RIP1) Kinase Specific Clinical Candidate (GSK2982772) for the Treatment of Inflammatory Diseases

Philip A. Harris, Scott B. Berger, Jae U Jeong, Rakesh Nagilla, Deepak Bandyopadhyay, Nino Campobasso, Carol A. Capriotti, Julie A Cox, Lauren Dare, Xiaoyang Dong, Patrick M Eidam, Joshua N. Finger, Sandra J Hoffman, James Kang, Viera Kasparcova, Bryan W. King, Ruth Lehr, Yunfeng Lan, Lara K Leister, John D Lich, Thomas T. MacDonald, Nathan A Miller, Michael T. Ouellette, Christina S. Pao, Attiq Rahman, Michael A. Reilly, Alan R. Rendina, Elizabeth J. Rivera, Michelle C Schaeffer, Clark A. Sehon, Robert R. Singhaus, Helen H. Sun, Barbara A. Swift, Rachel D Totoritis, Anna Vossenkamper, Paris Ward, David D Wisnoski, Daohua Zhang, Robert W Marquis, Peter J. Gough, and John J. Bertin

J. Med. Chem., **Just Accepted Manuscript** • DOI: 10.1021/acs.jmedchem.6b01751 • Publication Date (Web): 02 Feb 2017

Just Accepted

ACS Publications

Journal of Medicinal Chemistry is published by the American Chemical Society. 1155 Sixteenth Street N.W., Washington, DC 20036

	Zhang, Daohua; GlaxoSmithKline, Pattern Recognition Receptor DPU Marquis, Robert; GlaxoSmithKline, Medicinal Chemistry Gough, Peter; GlaxoSmithKline Bertin, John; GlaxoSmithKline

Discovery of a First-in-Class Receptor Interacting Protein 1 (RIP1) Kinase Specific Clinical Candidate (GSK2982772) for the Treatment of Inflammatory Diseases

Philip A. Harris,[†] Scott B. Berger,[†] Jae U. Jeong,[†] Rakesh Nagilla,[†] Deepak Bandyopadhyay,[‡] Nino Campobasso,[‡] Carol A. Capriotti,[†] Julie A. Cox,[‡] Lauren Dare,[†] Xiaoyang Dong,[†] Patrick M. Eidam,[†] Joshua N. Finger,[†] Sandra J. Hoffman,[†] James Kang,[†] Viera Kasparcova,[†] Bryan W. King,[‡] Ruth Lehr,[‡] Yunfeng Lan,[†] Lara K. Leister,[†] John D. Lich,[†] Thomas T. MacDonald,[#] Nathan A. Miller,[†] Michael T. Ouellette,[‡] Christina S. Pao,[‡] Attiq Rahman,[†] Michael A. Reilly,[†] Alan R. Rendina,[‡] Elizabeth J. Rivera,[†] Michelle C. Schaeffer,[‡] Clark A. Sehon,[†] Robert R. Singhaus,[†] Helen H. Sun,[†] Barbara A. Swift,[†] Rachel D. Totoritis,[‡] Anna Vossenkämper,[#] Paris Ward,[‡] David D. Wisnoski,[‡] Daohua Zhang,[†] Robert W. Marquis,[†] Peter J. Gough[†] and John Bertin[†]*

†Pattern Recognition Receptor DPU and ‡Platform Technology & Science, GlaxoSmithKline, Collegeville Road, Collegeville, Pennsylvania 19426, United States. #Centre for Immunobiology, Blizard Institute, Barts and The London School of Medicine and Dentistry, Queen Mary University of London, E1 2AD London, U.K.

ABSTRACT

RIP1 regulates necroptosis and inflammation and may play an important role in contributing to a variety of human pathologies, including immune-mediated inflammatory diseases. Small-molecule inhibitors of RIP1 kinase that are suitable for advancement into the clinic have yet to be described. Herein we report our lead optimization of a benzoxazepinone hit from a DNA-encoded library and the discovery and profile of clinical candidate GSK2982772 (compound **5**), currently in phase 2a clinical studies for psoriasis, rheumatoid arthritis and ulcerative colitis. Compound **5** potently binds to RIP1 with exquisite kinase specificity and has excellent activity in blocking many TNF-dependent cellular responses. Highlighting its potential as a novel anti-inflammatory agent, the inhibitor was also able to reduce spontaneous production of cytokines from human ulcerative colitis explants. The highly favorable physicochemical and ADMET properties of **5**, combined with high potency, lead to a predicted low oral dose in humans.

INTRODUCTION

RIP1 has emerged as an important upstream kinase that has been shown to regulate inflammation through both scaffolding and kinase specific functions.[1] As a critical regulator of inflammation, it is positioned as a key node in the innate immune response, which must be tightly regulated to maintain tissue homeostasis and can have detrimental consequences if dysregulated.[2,3] To this end, there is strong genetic evidence in humans and mice that mutations which shunt signaling down the RIP1 kinase pathway result in spontaneous and robust inflammation.[4-6] Recent work has shown that active RIP1 kinase can drive this inflammation through directly regulating programmed necrosis, the production of pro-inflammatory cytokines, inflammasome assembly and some forms of pathogenic apoptosis.[7-10] RIP1 has been shown to be

a critical driver of inflammation of various pathways downstream of the death receptors TNFR1, FasL and TRAIL, as well as toll-like receptors.[11-13] Hence blocking this pathway has the potential to result in a broad therapeutic benefit for multiple inflammatory diseases.

Degterev *et al.* were first to identify a series of RIP1 inhibitors using a phenotypic cell screen that measured their ability to block necrotic death induced by TNF and the caspase inhibitor zVAD.fmk.[14,15] The most advanced series, represented by indole-hydantoin **1** (known as Nec-1s or 7-Cl-O-Nec-1), was subsequently co-crystallized in the RIP1 kinase domain showing it to occupy an allosteric lipophilic pocket at the back of the ATP binding site.[16] This allosteric type III binding mode resulted in excellent kinase selectivity.[17] However, a narrow SAR profile coupled with moderate potency and poor pharmacokinetic properties for this series has limited their subsequent development to date.[18]

As part of our initial drug discovery efforts targeting RIP1 inhibitors we screened the library of GSK kinase inhibitors. This identified a number of potent inhibitors of RIP1 belonging to the type II class, targeting the "DFG-out" conformation of the kinase, as exemplified by **2** in Figure 1.[19] Further development of these type II inhibitors were hampered by high molecular weights and lipophilicities, coupled with low aqueous solubilities and a range of off-target kinase activities. From a separate high-throughput screen of the GSK compound collection we also identified 1-pivaloyl-5-phenyl 4,5-dihydropyrazole (**3**), known as GSK'963, a small, highly potent and selective RIP1 inhibitor. Although an excellent tool compound to study RIP1 inhibition in vitro**, 3** had minimal oral exposure in rodents limiting further development.[20]

From a third approach, screening of GSK's collection of DNA-encoded libraries[21] identified a potent and selective RIP1 inhibitor exemplified by benzoxazepinone **4**, known as GSK'481 (Figure 1).[22] This series differentiated itself over previously disclosed RIP1 inhibitors in that it

combined high RIP1 potency and kinase selectivity with potential to achieve oral exposure in rodents. Herein we describe the lead -optimization of this series that led to the identification of *(S)*-5-benzyl-*N*-(5-methyl-4-oxo-2,3,4,5-tetrahydrobenzo[b][1,4]oxazepin-3-yl)-1H-1,2,4-triazole-3-carboxamide **5** (GSK2982772). The high RIP1 potency, mono-kinase selectivity and excellent preclinical pharmacokinetic and developability profile of benzoxazepinone **5** led to its selection for development and it became the first-in-class RIP1 inhibitor to enter clinical trials in 2015 and recently completed phase 1 evaluation.

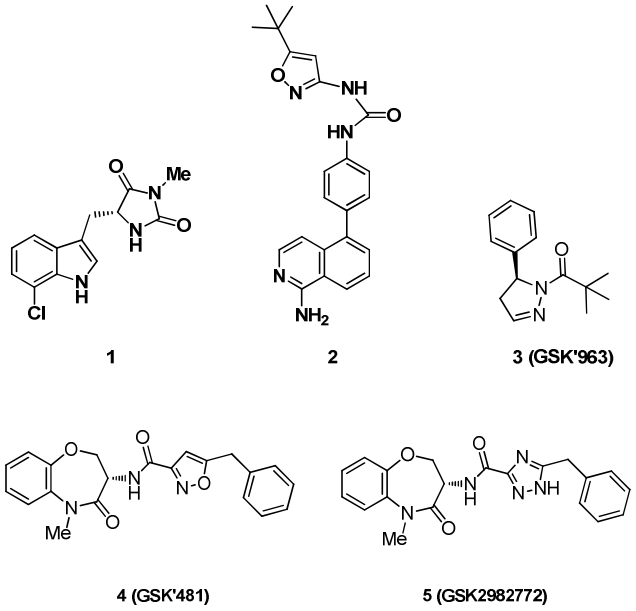

Figure 1. Structure of RIP1kinase inhibitors.

SAR AND LEAD OPTIMIZATION

The benzoxazepinone **4** hit identified from a DNA-encoded library screen possessed excellent potency in both a RIP1 (1-375) fluorescence polarization (FP) binding assay and an ADP-Glo functional biochemical assay (See Table 1).[22] Potency of **4** was maintained in a human

monocytic U937 cellular assay, measuring the ability to block necrotic cell death induced by treatment with TNF and the caspase inhibitor QVD-OPh. Remarkably for an unoptimized screening hit, benzoxazepinone **4** showed complete specificity for RIP1 kinase over all other kinases tested at 10 μM concentration when profiled against 318 kinases using a P33 radiolabeled assay screen at Reaction Biology Corp and 456 kinases using a competition binding assay KINOMEscan® at DiscoveRx Corp.[22] This high RIP1 enzymatic and cellular potency, coupled with complete kinase specificity made this series an excellent choice for further optimization into a RIP1 clinical candidate. This benzoxazepinone pharmacophore is to our knowledge a novel kinase inhibitor template. Our initial goals were to explore the SAR in RIP1 and identify a developable candidate that maintained the favorable in vitro profile, whilst optimizing three key parameters: lipophilicity, solubility and oral exposure in pre-clinical species. As a benchmark, benzoxazepinone **4** possessed high lipophilicity (log *D* = 5.9), low FaSSIF crystalline solubility (30 μg/mL) and a suboptimal pharmacokinetic profile. In rat **4** exhibited a low oral exposure ($AUC_{0-\infty}$ = 0.38 μg.h/mL at 2 mg/kg dose) coupled with a high clearance (69 mL/min/kg) and high volume of distribution (8.5 L/kg).

In the absence of a co-crystal structure, we relied on an homology model of the RIP1 to predict how this series was binding in the ATP binding pocket.[22] This model had the lactam carbonyl of the benzoxazepinone and the exocyclic NH making hydrogen-bond interactions with the kinase hinge at Met95 and Glu93, respectively. Our early SAR investigations began around this putative hinge binding region. Removal of the lactam *N*-methyl group gave analog **6** with about a log drop in enzyme and cell potencies as shown in Table 1, but very encouragingly a substantial increase in rat oral exposure ($AUC_{0-\infty}$ 2.2 μg.h/mL at 2 mg/kg dose) accompanied this change.[22] However, increasing the size of the *N*-substituent to the corresponding ethyl or cyclopropyl

analogs **7** and **8** led to a rapid loss in potency. The *S* chiral center was established as important for binding, as the *R* enantiomer **9** and α-methylation of the chiral carbon leading to **10** were both inactive. Methylation of the exocyclic NH (benzoxazepinone **11**) or removal of the benzoxazepinone carbonyl to give benzoxazepine **12** both led to complete loss of activity. At the conclusion of this lead optimization a co-crystal structure of **5** was obtained in RIP1 as discussed later in this article. Interestingly, this revealed the series does not make any interaction with the kinase hinge, rather the inhibitor sits deeper in the ATP binding pocket, the benzyl group occupying an allosteric lipophilic pocket at the back. The benzoxazepinone moiety resides in a tight pocket formed by two β-strands defined by Leu90-Val91-Met92 and Ile43-Met44-Lys45 (see Figure 2). Changes that increase size at either the lactam nitrogen (e.g. **7**, **8**) or chiral center (e.g. **10**, **11**), or alter the conformation of the 7-membered ring (e.g. **9**, **12**), are not tolerated.

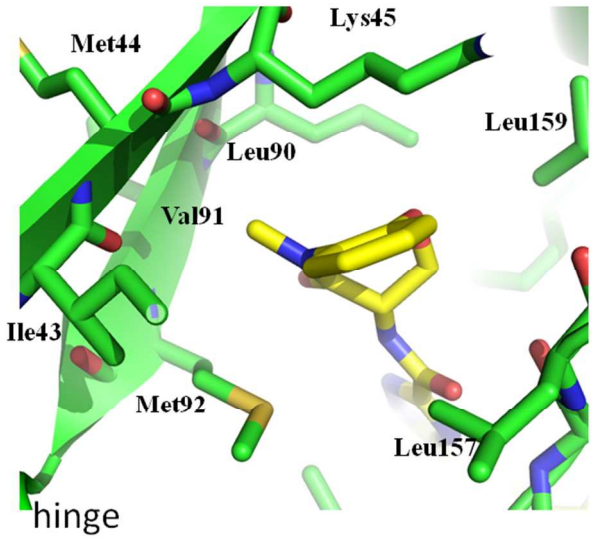

Figure 2. Crystal structure of compound **5** (yellow) in the RIP1 kinase domain (green) with the benzoxazepinone packed against 2 β-strands defined by Leu90-Val91-Met92 and Ile43-Met44-Lys45.

Table 1. SAR around the lactam amide and chiral center[a]

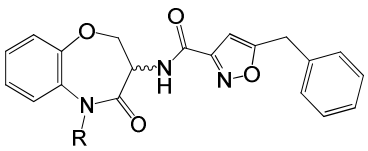

4, 6-8 (S enantiomer)
9 (R enantiomer)

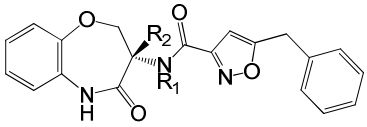

10 (R_1 = H, R_2 = Me)
11 (R_1 = Me, R_2 = H)

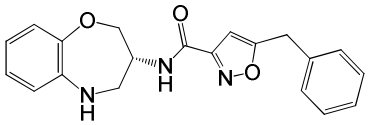

12

Cpd	R	R_1	R_2	RIP1 FP[b] IC_{50} (nM)	ADP-Glo[c] IC_{50} (nM)	U937 IC_{50} (nM)
4	Me	–	–	10	1.6	10
6	H	–	–	32	16	200
7	Et	–	–	3,162	–	7,943
8	CyPr[d]	–	–	>10,000	–	>10,000
9	H	–	–	>10,000	–	>10,000
10	–	H	Me	>10,000	–	>10,000
11	–	Me	H	>10,000	–	>10,000
12	–	–	–	>10,000	–	>10,000

[a]Assay protocols are described in Supporting Information; IC_{50} values are the average of at least two determinations. [b]Lower limit of sensitivity is ca. 10 nM. [c]Conventional data analysis was used for less potent inhibitors (IC_{50} > 10 nM); whereas tight binding analyses was used for more potent inhibitors (IC_{50} < 10 nM). [d] Cyclopropyl

A survey of various replacements for the heteroatom of the benzoxazepinone was carried out involving synthesis of the benzothiazepinone **13**, benzazepinone **14**, and benzodiazepinones **15**

and **16** analogs (see Table 2). This heterocycle switch maintained the high RIP1 in vitro potency, presumably because it maintained the required conformation of the seven-membered ring. Indeed benzothiazepinone **13** was extremely potent in the ADP-Glo assay (IC_{50} = 63 pM), but had no rat oral exposure. The benzodiazepinone **15** did moderately improve lipophilicity, FaSSIF solubility (97 μg/mL) and rat oral exposure compared to benzoxazepinone **4**.

Table 2. Replacements of benzoxazepinone heteroatom[a]

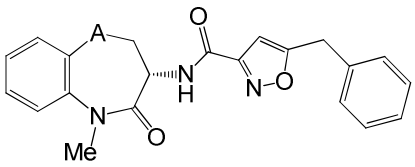

Cpd	A	ADP-Glo[b] IC_{50} (nM)	U937 IC_{50} (nM)	$AUC_{0-\infty}$[c] μg.h/mL	log *D*[d]
4	O	1.6	10	0.38	5.9
13	S	0.063	2	BLD[d]	6.2
14	CH_2	0.20	6.3	0.007	6.0
15	NH	0.79	40	0.80	5.0
16	NMe	5.0	20	0.082	6.0

[a]Assay protocols are described in Supporting Information; IC_{50} values are the average of at least two determinations. [b]ADP-Glo tight binding analyses was used as the lower limit of sensitivity was reached in the RIP1 FP assay. [c]Rat oral exposure at 2 mg/kg. [d]Below level of detection. [d]CHI (chromatographic hydrophobicity index) log *D* at pH 7.4 was calculated from the retention time (t_R) observed in a fast gradient reverse-phase HPLC.[23]

More substantial modifications of the benzoxazepinone ring were also explored. Expanding the heterocycle to an eight-membered benzo[1,4]oxazocinone **17**, or contracting to a quinolinone **18**, both lost potency. Similarly removal of the benzo function to yield a 1,4-oxazepan-5-one **19** or

its saturation to a cyclohexyl ring **20** resulted in inactive analogs (see Table 3). These findings fit with the co-crystal structure of **5** in RIP1 in which the benzoxazepinone moiety occupies a tight pocket, see Figure 2, and is therefore not amenable to modifications that significantly alter the oxazepinone conformation.

Table 3. Modifications of benzoxazepinone heterocycle[a]

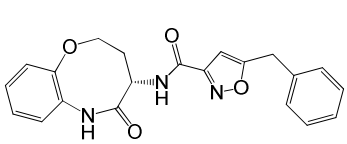

17

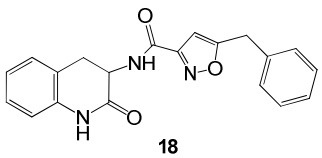

18

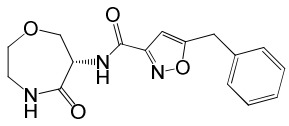

19

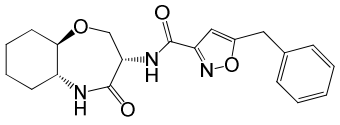

20

Cpd	RIP1 FP IC_{50} (nM)	U937 IC_{50} (nM)	$AUC_{0-\infty}$[b] μg.h/mL
6	32	200	2.2
17	200	631	0.38
18	>10,000	>10,000	–
19	>10,000	>10,000	–
20	>10,000	–	

[a]Assay protocols are described in Supporting Information; IC_{50} values are the average of at least two determinations. [b]Rat oral exposure at 2 mg/kg.

Substitution at the aryl ring of the benzoxazepinone ring was also investigated revealing a good tolerance for substitution at the 7- and 8-positions, which in the co-crystal structure are orientated towards solvent exposed space. The 6 and 9-positions had less room for substitutions, with only fluorine well tolerated. As shown for selected representative examples in Table 4, *N*-

acetyl (**21**), *N*-methyl formate (**22**) or *N*-methyl sulfonyl (**23**) 7-substitutions, or attachment of heterocycles such as pyrazole (**24**) or 1,3,4-oxadiazol-2-one (**25**), all maintained comparable potencies. In particular, the 1,3,4-oxadiazol-2-one (**25**) possessed good rat total oral exposure and improved lipophilicity (log *D* = 4.4), but suffered from a low FaSSIF solubility (8 μg/mL).

Table 4. 7-Substitutions at the benzoxazepinone[a]

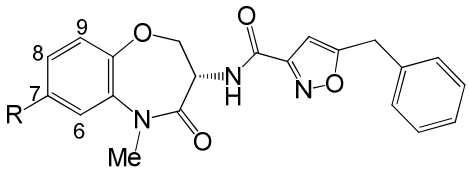

Cpd	Substitution	ADP-Glo[b] IC_{50} (nM)	U937 IC_{50} (nM)	$AUC_{0-\infty}$[c] μg.h/mL
4	H	1.6	10	0.38
21	NHCOMe	0.32	7.9	0.45
22	$NHCO_2Me$	0.32	10	1.1
23	$NHSO_2Me$	0.63	13	-
24	3-pyrazole	1.0	6.3	0.60
25	5-(1,3,4-oxadiazol-2-one)	0.5	3.2	2.1

[a]Assay protocols are described in Supporting Information; IC_{50} values are the average of at least two determinations. [b]ADP-Glo tight binding analyses was used as the lower limit of sensitivity was reached in the RIP1 FP assay. [c]Rat oral exposure at 2 mg/kg

The SAR around the benzyl group, which resides in an allosteric hydrophobic pocket at the back of the ATP binding site (see Figure 4), was quite narrow and clearly favored lipophilic groups, as shown in Table 5. Removal of the phenyl group (analog **26**) resulted in loss of activity, and suboptimal activity resulted from replacement of phenyl with n-butyl (**27**), isopropyl (**28**) or cyclohexyl (**29**) groups. Any substitutions at the phenyl ring other than fluorine

were detrimental to potency, and introduction of polarity such as the *N*-piperidine functionality (analog **30**) were not tolerated.

Table 5. Modifications of benzyl group[a]

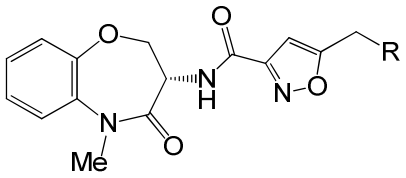

Cpd	R	RIP1 FP IC_{50} (nM)	U937 IC_{50} (nM)
4	Ph	10	10
26	H	12,600	–
27	nBu	100	126
28	iPr	1,600	6310
29	cyclohexyl	251	501
30	*N*-piperidine	>10,000	>10,000

[a]Assay protocols are described in Supporting Information; IC_{50} values are the average of at least two determinations.

Ultimately it was replacement of the isoxazole heterocycle that had the greatest overall impact on improving the developability profile of this series. The choice of heterocycle had a significant effect on potency, as shown for selected examples in Table 6. A general trend, although not absolute, was for heterocycles with a "non-bridging" nitrogen ortho to the amide carbonyl to possess optimal potency. For example, oxazole **31** (IC_{50} = 50 pM) is much more potent than its isomer **33** (IC_{50} = 794 nM), and the imidazole **35** (IC_{50} = 0.4 nM) is much more active than its isomer **34** (IC_{50} = 1.3 μM) or pyrazole analog **36** (IC_{50} = 63 nM). This nitrogen adjacent to the

carbonyl may be imparting a favorable trans orientation due to electron lone pair repulsion separating the negatively charged nitrogen and amide oxygen atoms thus positioning the benzyl group optimally into the tight back pocket.[24] Thiazole **32**, with low activity, appears to be an anomaly to this trend, but likely the large size of the sulfur atom is altering orientation of the benzyl group resulting in an suboptimal fit into the back pocket. The *N*-benzyl-1,2,3-triazole **40** displayed encouragingly improved rat oral exposure compared to its *N*-benzyl-1,2-4-triazole isomer **41**, but the breakthrough came with preparation of the 3-benzyl-1,2-4-triazole isomer **5**, which had the optimal combination of in vitro potency, lipophilicity (log *D* 3.8) and rat oral exposure ($AUC_{0-\infty}$ 2.3 μg.h/mL at 2 mg/kg dose). As can be seen from Figure 3 there is a clear correlation between lower lipophilicity (log $D < 4.3$)[23] and improved kinetic aqueous solubilities for the compounds profiled in this paper.[25] A recent study of heterocycle containing molecules in drug developability assays found that 1,2,4-triazoles possessed optimal profiles including solubility.[26] Presumably the lower lipophilicity and increased solubility of **5** resides in an optimal charge distribution of the 1,2,4-trizaole leading to larger dipole moment (calculated dipole moment for the unsubstituted 4*H*-1,2,4-triazole is 5.81 Debye).[27] Adding an additional nitrogen resulted in the tetrazole analog **42**, which possessed excellent potency but suboptimal lipophilicity and oral exposure. Replacing the heterocycle with a 1,3-phenyl analog **43** resulted in loss of considerable potency, although this could be recovered by introduction of an ortho nitrogen as shown in pyridine **44**. However both analogs are quite lipophilic, with correspondingly poor solubilities. The lead optimization culminated in selection of **5** to progress into development based on the inhibitor maintaining the excellent potency and kinase selectivity of the lead **4**, combined with a significantly improved developability profile. This was demonstrated by a two log improvement in log *D* and 7-fold improvements in oral exposure in

rat of **5** compared to **4** (see Table 6). We identified a stable non-solvated crystalline form of **5** with a low melting point (131 °C) and improved FaSSIF solubility (230 μg/mL). As discussed later in the section on preclinical characterization of **5**, this resulted in an excellent dose proportionality profile in both pharmokinetic and safety studies across a large dose range (2 to 1000 mg/kg).

Table 6. Heterocycle replacements[a]

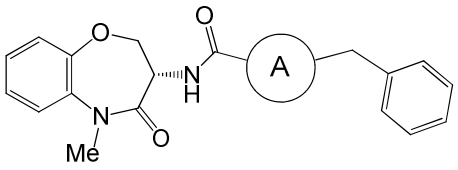

Cpd	A	FP/ADP-Glo[b] IC_{50} (nM)	U937 IC_{50} (nM)	log *D*[c]	$AUC_{0-\infty}$[d] μg.h/mL
4	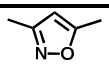	1.6	10	5.9	0.38
31	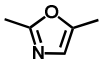	0.05	1.0	5.6	0.055
32	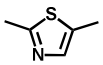	631	794	6.5	–
33	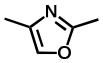	794	2,512	5.4	–
34	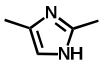	1,259	1,995	3.8	–
35	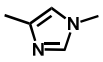	0.4	6.3	4.2	0.66
36	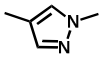	63	631	4.0	2.9
37	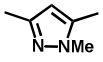	0.4	10	5.4	0.17
38	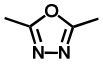	0.79	7.9	4.9	0.13

39	0.5	5.0	5.4	0.033
40	1.0	25	4.6	1.3
41	0.63	1.6	4.2	0.28
5	1.0	6.3	3.8	2.3
42	0.079	2.5	5.0	0.24
43	251	398	6.3	–
44	2	40	6.4	–

[a]Assay protocols are described in Supporting Information; IC_{50} values are the average of at least two determinations. [b]RIP1 FP binding assay was used to assess potency of inhibitors with IC_{50} > 10 nM; whereas for more potent inhibitors where the limit of sensitivity FP assay was reached (ca 10 nM) the ADP-Glo tight binding analyses was employed to more accurately determine potency. A good correlation was observed between both assay formats. [c]CHI (chromatographic hydrophobicity index) log *D* at pH 7.4 was calculated from the retention time (t_R) observed in a fast gradient reverse-phase HPLC.[23] [d]Rat oral exposure at 2 mg/kg.

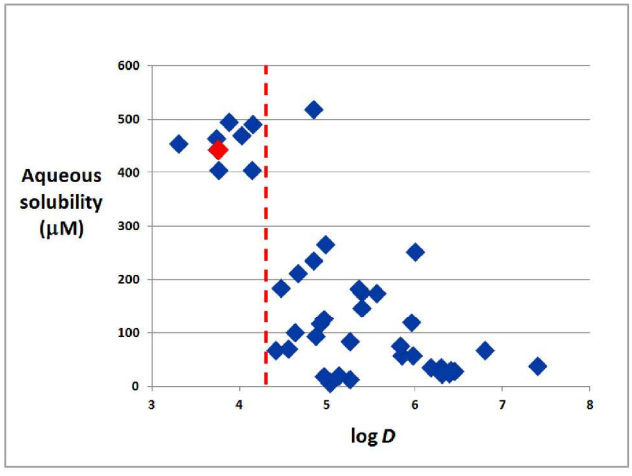

Figure 3. Comparison of chromatographic hydrophobicity index (CHI) log *D* and aqueous solubility for inhibitors **4-45**. Reducing lipophilicity, specifically with a log *D* < 4.3 (indicated by red line), leads to higher aqueous solubilities. Benzoxazepinone **5** is colored red. CHI log *D* at

pH 7.4 was calculated from the retention time (t_R) observed in a fast gradient reverse-phase HPLC.[23] Kinetic aqueous solubility was measured by chemiluminescence nitrogen detection (CLND) from phosphate buffer saline pH 7.4 solution, prepared from DMSO stock solution of the inhibitor.[25]

BINDING MODE AND KINASE SELECTIVITY

Subsequent to the identification of **5** as a development candidate we were able to co-crystallize this template in RIP1. This was achieved by reproducing the published co-crystal structure of Necrostatin-4 (*(S)-N*-(1-(2-chloro-6-fluorophenyl)ethyl)-5-cyano-1-methyl-1H-pyrrole-2-carboxamide) bound to the RIP1 construct (1–294, C34A, C127A, C233A, and C240A) and displacing Necrostatin-4 with benzoxazepinone **5**.[16] The X-ray structure of the RIP1 kinase domain was refined to 2.6 Å resolution (see Figure 4a). In this structure, benzoxazepinone **5** was observed to be buried deep in the pocket between the *N*-terminal and C-terminal domains. Interestingly the molecule resides further in the binding pocket than we initially modeled making no interaction with the hinge residues. The triazole and benzyl functionality of **5** occupies the same allosteric lipophilic pocket at the back of the ATP binding site as Necrostatin-4 (Figure 4b), suggestive more of a type III class of kinase inhibitor.[28] Although inhibitor **5** does not occupy the same space as the adenine ring of ATP, the benzoxazepinone ring does occupy space where the alpha phosphate would reside so the inhibition is not strictly allosteric. The amide carbonyl attached to the triazole makes a direct hydrogen-bond interaction with the backbone amide NH of Asp156. The triazole nitrogen makes a water-mediated hydrogen-bond to the carbonyl oxygens of Met67 and Val76. The C-helix is shifted compared to the bound **1** structure and the activation loop is more ordered when **5** is bound. Structure determination was done by molecular

replacement using the atomic coordinates of RIP1 kinase domain with Necrostatin-4 (PDB code 4ITJ) as a search model (see Supplemental Information for details).

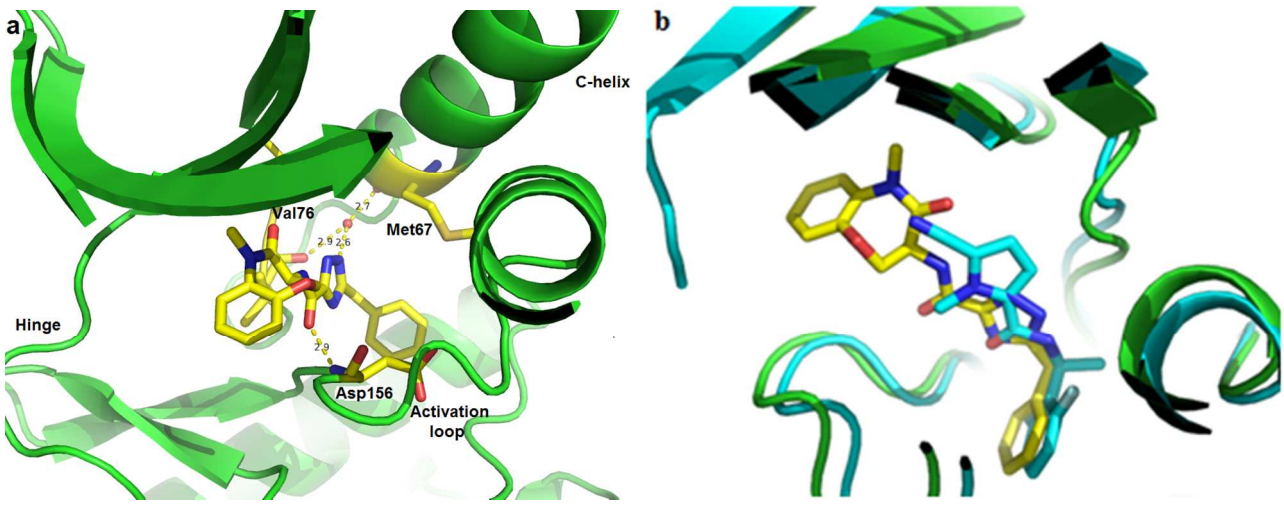

Figure 4. (a) Co-crystal structure of RIP1 (1–294, C34A, C127A, C233A, and C240A) and benzoxazepinone **5**. (b) Overlaid crystal structures of compound **5** (yellow) in the RIP1 kinase domain (green) with Necrostatin 4 (cyan) in the RIP1 kinase domain (cyan)

The type III binding mode observed for this pharmacophore in RIP1 results in complete kinase selectivity as exemplified by the kinase profile of **5** against both a P33 radiolabeled assay screen at Reaction Biology Corp (339 kinases) and a competition binding assay KINOMEscan at DiscoveRx Corp (456 kinases). In both assays benzoxazepinone **5** was tested at a concentration of 10 μM, which represents an estimated >10,000 fold selectivity window based on the RIP1 ADP-Glo potency of 1 nM. The Reaction Biology Corp kinase dendrogram is shown in Figure 5. Details on both profiles are available in the Supporting Information section. This mono-kinase selectivity profile was not observed with any of the type II DFG-out RIP1 inhibitors we profiled.[19]

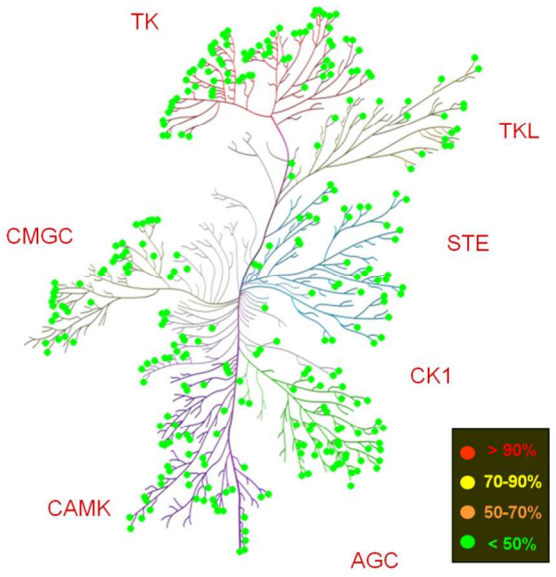

Figure 5. Kinase selectivity profile of compound **5** as shown by a Reaction Biology Core kinase panel screen against 339 kinases assayed at 10 μM in duplicate. Compound selectivity is represented in a dendrogram view of the human kinome phylogenetic tree. All kinases tested were inactive (< 50%) as indicated by green circles. RIP1 was not part of this panel.

PRECLINICAL CHARACTERIZATION

As would be predicted by the co-crystal structure, benzoxazepinone **5** is an ATP competitive inhibitor (see Supporting Information). The binding kinetics are similar to benzoxazepinones recently profiled, with a moderate on-rate constant (k_{on} = 0.045 $\mu M^{-1}sec^{-1}$), accompanied by a slow off-rate constant k_{off} = 0.37 $hour^{-1}$ ($t_{1/2}$ = 112 min), measured by stopped-flow kinetics and FP competitive binding, respectively (see Supporting Information). In addition to efficacy against the immortalized U937 human monocyte cell line, activity of **5** was also assessed in primary neutrophils isolated from human whole blood. In this assay TNF is co-incubated with both the caspase inhibitor QVD-OPh and the SMAC mimetic RMT 5265, which block the

apoptosis and NF-κB pathways, respectively, driving the TNF response down the necrosis pathway.[29] Inhibitor **5** was able to potently block this response as shown by determination of overall cell viability as measured by cellular ATP levels (IC_{50} = 1.6 nM), cell death as measured by LDH release (IC_{50} = 0.4 nM) and RIP1-dependent inflammatory cytokine MIP-1β production, either as absolute levels for protein, or fold changes in mRNA expression (IC_{50} = 0.5 nM).

A human whole blood stimulation assay was developed in which the necroptosis pathway is activated in a similar fashion through stimulation with TNF co-incubated with the caspase inhibitor QVD-OPh or zVAD.fmk, and the SMAC mimetic RMT 5265. In this assay benzoxazepinone **5** was also shown to be very potent as measured by inhibition of cytokine MIP-1β ((IC_{50} = 2 nM). In a similar cynomolgus monkey whole blood stimulation assay, benzoxazepinone **5** was equally efficacious (IC_{50} = 4 nM).

In addition to examining potency in stimulated cellular systems, benzoxazepinone **5** was also able to reduce spontaneous production of cytokines (IL-1β and IL-6) in a concentration-dependent fashion from ulcerative colitis explant tissue in overnight incubations (Figure 6). As previously described, intestinal mucosal tissue obtained from inflamed areas of the gut spontaneously release significantly elevated levels of inflammatory cytokines compared to healthy mucosa, recapitulating the inflammatory phenotype found in vivo.[30] Although this human biopsy assay has a high degree of inter subject variability and response rate, the responses are similar to the steroid positive control prednisolone. The corresponding *R* enantiomer **45**, inactive against RIP1, was included as a negative control. Although the variability in the data makes accurate calculation of potency difficult, the data are consistent with the potency of **5** in other cell-based assays.

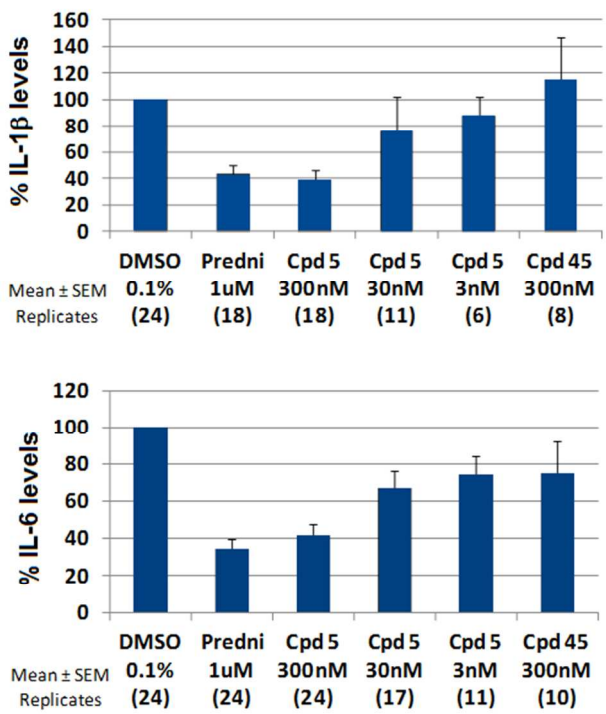

Figure 6. Inhibition of overnight IL-1β and IL-6 production in human explant samples taken from ulcerative colitis patients for benzoxazepinone **5** in comparison to prednisolone (predni) and the corresponding RIP1 inactive *R* enantiomer **45**.

We previously reported this series demonstrates a species selectivity for inhibition of primate RIP1 compared to non-primate RIP1.[22] Consistent with this observation, compound **5** exhibited approximately equivalent RIP1 FP potency against human and monkey RIP1, but was significantly less potent against non-primate RIP1, as shown in Table 7. This species selectivity was not observed with any of the type II DFG-out RIP1 inhibitors we previously profiled (for example **2**), but appears to be reserved for this type III binding mode.[19] This reduced biochemical potency also translated to reduced mouse cellular efficacy, as evidenced by a 340 fold reduction in cellular potency for compound **5** in blockage of the necrotic death (induced by

TNF and QVD-OPh) in murine fibrosarcoma L929 cells (IC_{50} = 1.3 μM), compared to human monocytic U937 cells (IC_{50} = 0.0063 μM). As detailed in our prior report, selectively mutating key amino acids in the mouse RIP1 activation loop, where non-primate differed from primate, increases the potency of benzoxazepinone **4** in mouse cells to that approaching human.[22] This suggests that the activation loop is the key region in murine RIP1 responsible for the lower efficacy against this series. We speculate that the differences in amino acid sequence cause murine RIP1 to have reduced flexibility in adopting the activation loop conformation required for this inhibitor to bind in its preferred type III conformation.

Table 7. RIP1 species selectivity of compound **5**

Species	RIP1 FP IC_{50} (μM)	Fold
Human	0.016[a]	1
Monkey	0.020[a]	1.25
Rabbit	0.79	49
Rat	2.0	125
Mouse	2.5	156
Dog	5.0	313
Minipig	>10	>625

[a]Values at the lower limit of sensitivity (ca. 10 nM).

The ability to explore an in vitro to in vivo correlation has been limited to acute models, as the reduction in rodent RIP1 potency meant assessment in more long-term disease models has not been possible. We had sufficient potency and exposure to evaluate benzoxazepinone **5** in an acute in vivo mouse model evaluating protection from TNF induced lethal shock, which has been

shown to be RIP1 kinase dependent.[31] In this model, injection of TNF leads to a systemic inflammatory response, characterized by hypotension, hepatitis, hypothermia and bowel necrosis over 6-7 hours. In a similar model, injection of TNF combined with the caspase inhibitor zVAD leads to a similar but earlier onset systemic inflammatory response in about 3 hours. Efficacy can be measured by the ability of the RIP1 inhibitor to prevent body temperature loss. Benzodiazepinone **5** was dosed orally 15 min prior to TNF and showed 68, 80 and 87% protection from temperature loss over 6 hours, at doses of 3, 10 and 50 mg/kg, respectively (Figure 7). In the corresponding TNF/zVAD model, benzodiazepinone **5** showed 13, 63 and 93% protection from temperature loss over 3 hours. Assuming the efficacy is C_{max} driven, the correlation of change in body temperature, combined with the estimated blood drug level at the time of the challenge, leads to an estimated IC_{50} of 1 and 3.2 μM for both models (Figure 8). This aligns closely with the in vitro assessment of RIP1 mouse L929 cellular activity of **5** (IC_{50} = 1.3 μM).

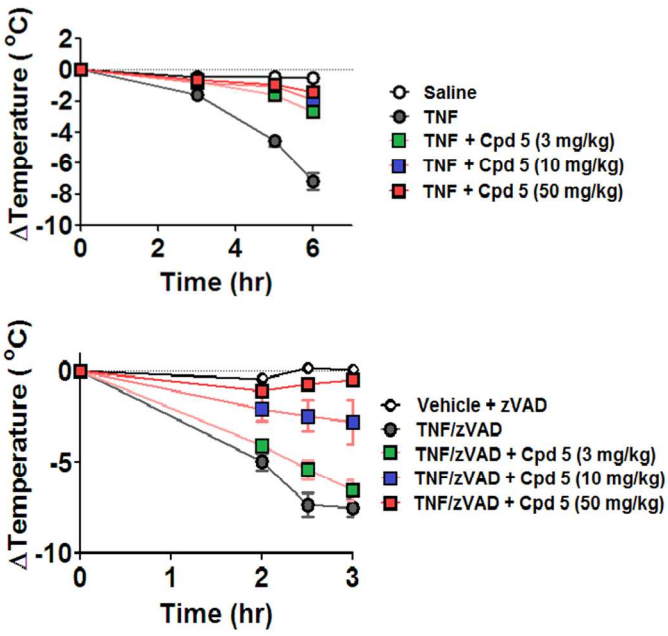

Figure 7. Evaluation of benzodiazepinone **5** in the TNF (top) and TNF/zVAD (bottom) induced lethal shock mouse models, measuring reduction in body temperature loss over time.

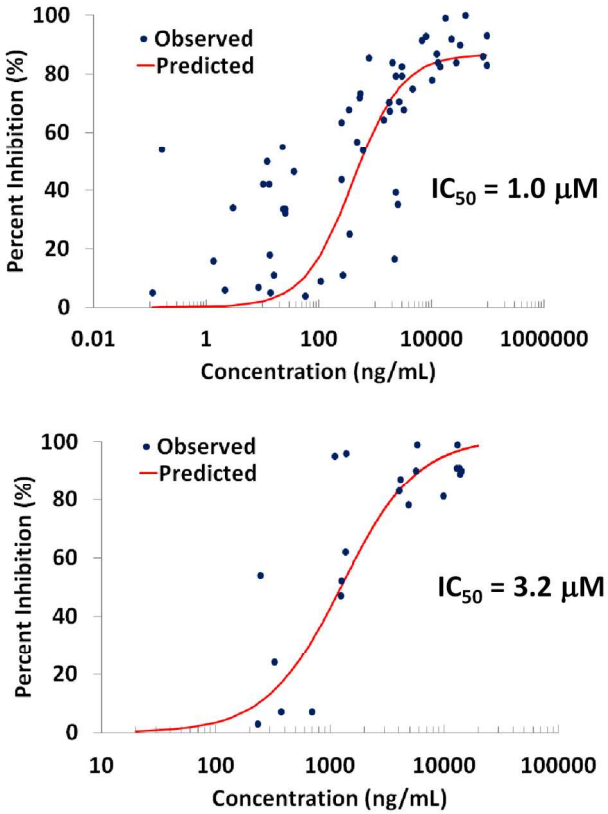

Figure 8. Dose response curves for benzodiazepinone **5** in the TNF (top) and TNF/zVAD (bottom) mouse induced lethal shock models.[a]

[a]Terminal blood concentrations were quantified in the study animals. For each individual animal, a theoretical Cmax was calculated using Cmax and concentration at 3 h from satellite animals. These estimated Cmax values were then used to build the dose response model.

The assumption that the inhibition in the TNF/zVAD model can be approximated to a direct effect was assessed by orally dosing **5** at 50 mg/kg and then altering the time of the TNF/zVAD challenge over a 16 hour period. The measured levels of inhibition of temperature loss were then compared to the expected levels of inhibition predicted from the oral pharmacokinetic profile and the standard TNF/zVAD model. As shown in Figure 9, the levels of observed inhibition correlated reasonably well with the levels of predicted inhibition, and hence the assumption that the model can be approximated to a direct effect is likely valid within the variability of the assay.

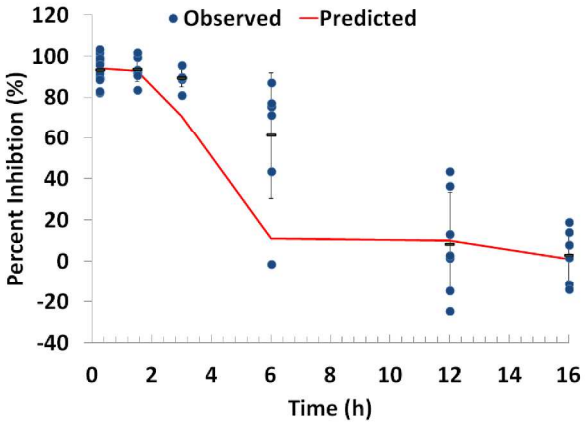

Figure 9. Comparison of predicted and actual inhibition of temperature drop following a 50 mg/kg oral dose of **5** in the mouse at various times of TNF/zVAD challenge over 16 hours.

Benzoxazepinone **5** displayed a good free fraction in blood in rat (4.2%), dog (11%), cynomolgus monkey (11%) and human (7.4%). The inhibitor had a good pharmacokinetic profile across both rat and monkey (see Table 8). In vitro comparisons of the metabolic stability of **5** in microsomes and hepatocytes showed it was stable across all species measured including human (see Supporting Information). All the Phase I and Phase II biotransformations observed in human

were also measured in rat and monkey hepatocytes, as shown in Figure 10. The tissue distribution of **5** in rats was evaluated following iv infusion over 4 hours before a range of terminal tissue samples were taken and parent drug concentrations determined and compared to blood levels (see Supporting Information). This study showed that **5** distributed into a range of tissues including colon, liver, kidney and heart at concentrations comparable to blood. However, **5** had low brain penetration in rat (4%) despite possessing good cell permeability (21 x 10^{-6} cm/s), which is likely due to active extrusion of **5** from brain via the efflux drug transporter P-glycoprotein (Pgp) (see Supporting Information).

Table 8. Pharmacokinetic Parameters of 5 after Intravenous or Oral Administration to Rats and Cynomolgus Monkeys

Route	Parameter	Rat	Monkey
iv	dose (mg/kg)	1.1	1.2
	Cl (mL/min/kg)	17 ± 5	10 ± 3
	Vdss (L/kg)	2.7 ± 0.6	2.2 ± 0.9
	$t_{1/2}$ (h)	3.9 ± 0.7	6.5 ± 1.0
po	dose (mg/kg)	2.1	1.9
	T_{max} (h)	0.25 ± 0.0	1.8 ± 1.1
	C_{max} (μg/mL)	810 ± 160	720 ± 240
	AUC (μg·h/mL)	2.3 ± 0.8	2.9 ± 0.8
	bioavailability (%)	110 ± 20	86 ± 6

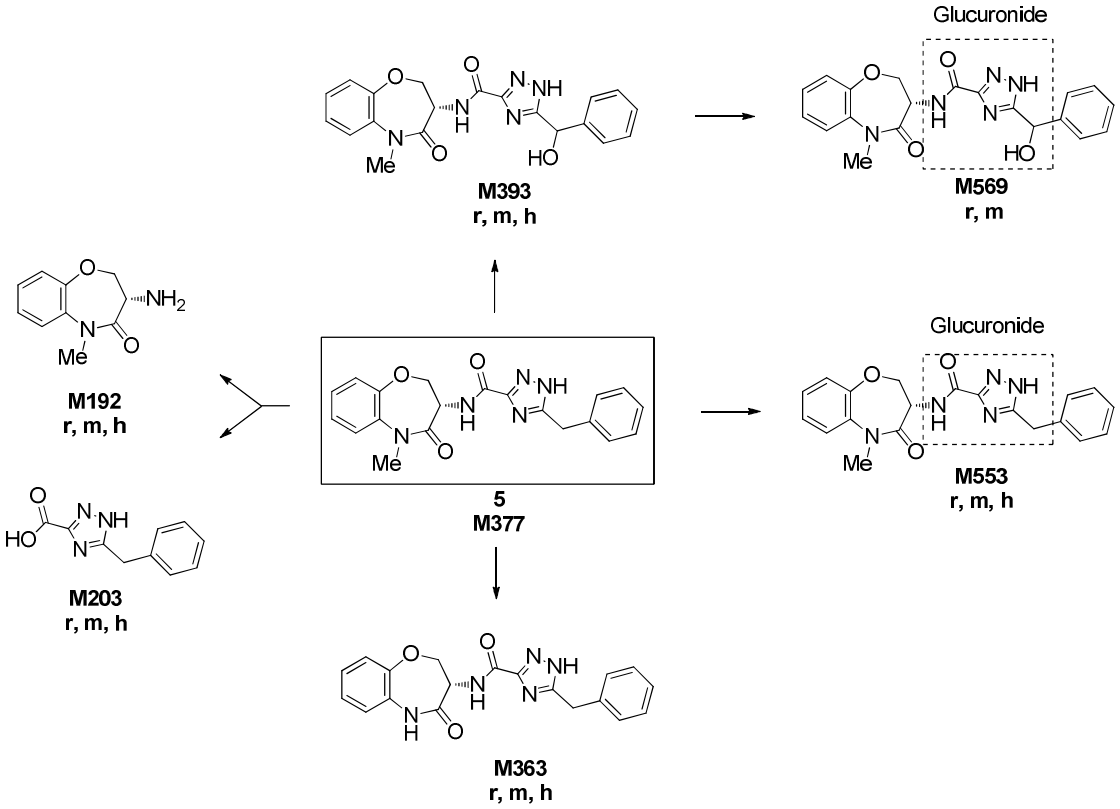

Figure 10. Summary of metabolites of **5** following incubations with cryopreserved hepatocytes from rats (r), cynomolgus monkeys (m) and humans (h). Compound **5** (10 μM) was incubated in a hepatocyte suspensions (1 million cells/mL) at 37°C for up to 4 hours under 5% CO_2:95% O_2.

Allometric scaling and in vitro to in vivo extrapolations (using GSK proprietary software) with and without effects of free fraction were used to generate predictions of the human pharmacokinetic parameters of **5** (Table 9). These showed a high level of correlation and predicted **5** to have high bioavailability, moderate to low clearance with a moderate volume and a terminal half life in the order of 12 hours. The average clearance and volume values were then used to reconstruct a mono-exponential predicted human blood concentration time profile as shown in Figure 11.

Table 9. Average predicted human PK profile of benzoxazepinone **5** based on allometry and in vitro to in vivo extrapolation.

Parameter	Average	95%	-95%
Clearance (mL/min/kg)	6.3	7.4	5.2
Volume (L/kg)	2.5	2.7	2.2
Half life (h)	11.5	13.5	9.5
Bioavailability (%)	79	86	72

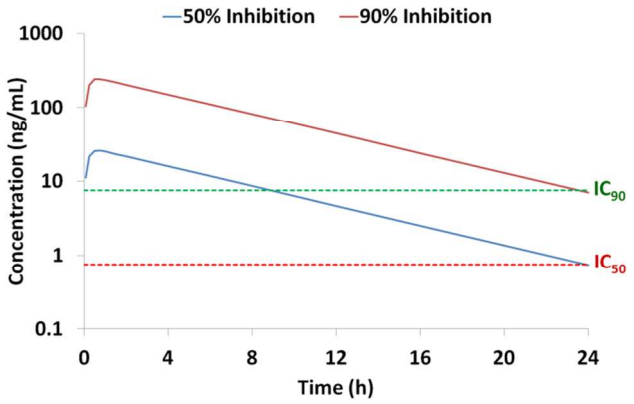

Figure 11. Predicted human blood concentration time profile of benzoxazepinone **5** overlaid with the human whole blood inhibition IC_{90} and IC_{50} concentrations

Human PK/PD was modeled using the predicted human PK profile along with a series of in vitro activity assays. Calculations were made with and without taking into account differences in free fraction across species, although the lack of apparent shift between binding, cellular and whole blood numbers makes the true impact of free fraction difficult to interpret. Doses were

then scaled and modeled to achieve 50 and 90% inhibition over 24 hours, as illustrated in Figure 12. Without a clear model to link the required level of inhibition to a validated disease model, our initial clinical target was to maintain a 90% effect level over 24 hours. Using inhibition of human whole blood, **5** is predicted to require a 60 mg dose once a day to achieve a greater than 90% pharmodynamic effect over 24 hours with an AUC of 1.7 μg·h/mL.

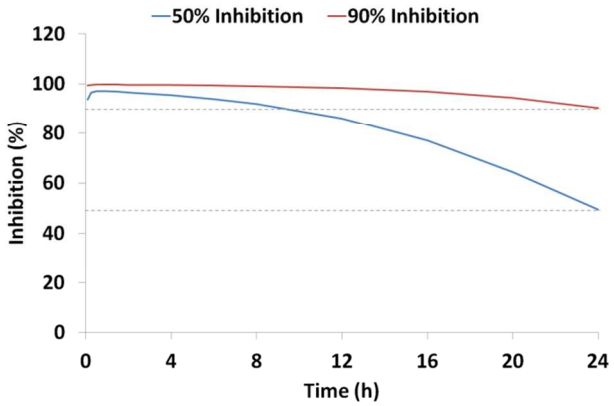

Figure 12. Predicted human PD dose effect levels of benzoxaepinone **5** at 6.3 and 60 mg once daily, achieving 50 and 90% RIP1 inhibition levels over 24 hours, respectively.

Compound **5** demonstrated a clean profile against a range of non-kinase targets. In particular no inhibitory potential was observed towards recombinant human cytochrome P450 (CYP) enzymes, with the exception of weak activity against CYP2C9 (IC_{50} = 25 μM). Compound **5** produced a weak concentration-dependent inhibition of hERG in human embryonic kidney (HEK-293) cells, with an estimated IC_{50} of 195 μM, and also showed a weak activation of the human Pregnane X receptor (hPXR) with an EC_{50} of 13 μM.

The non-solvated crystalline form of **5** has a predicted pKa of 7.7 for the triazole NH and an aqueous solubility of approximately 0.1 mg/mL across the physiological pH range. The optimized crystalline solubility of **5** led to excellent dose proportionality comparing solution and suspension oral dosing ranging from 2 to 1000 mg/kg in both rat and cynomolgus monkey (Figure 13). This dose proportionality allowed us to evaluate compound **5** across a wide dose range for pre-clinical toxicity studies. Due to the significantly lower potency for this series against non-primate RIP1, cynomolgus monkey was selected as the second species for pre-clinical safety evaluation. One month safety assessment in rat and monkey provided ample safety windows to facilitate progression of **5** into phase 1 clinical trials.

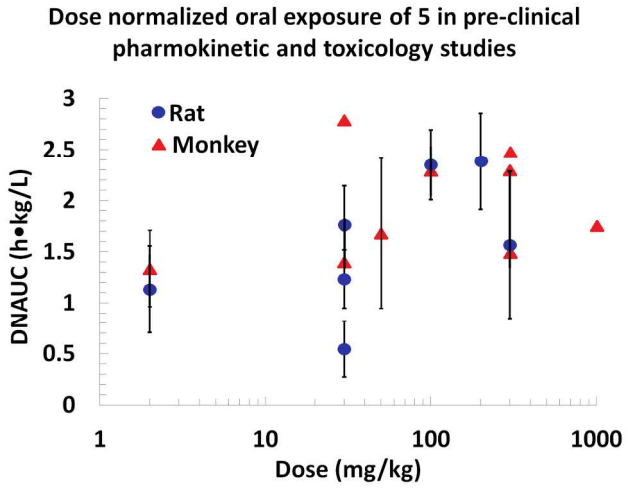

Figure 13. Dose proportionality for **5** in rat and cynomolgus monkey following oral dosing in pharmacokinetic and toxicology studies, as measured by dose normalized AUC (DNAUC).

CHEMISTRY

The general route to prepare this benzoxazepinone template has been described previously starting from BOC-L-serine and is detailed in Scheme 1.[22] The preparation of the corresponding

benzthiazepinone and benzodiazepinone analogs have also been described previously and involve substituting the BOC-L-serine with BOC-L-cysteine or 3-amino-BOC-L-alanine, respectively.[22]

Scheme 1.

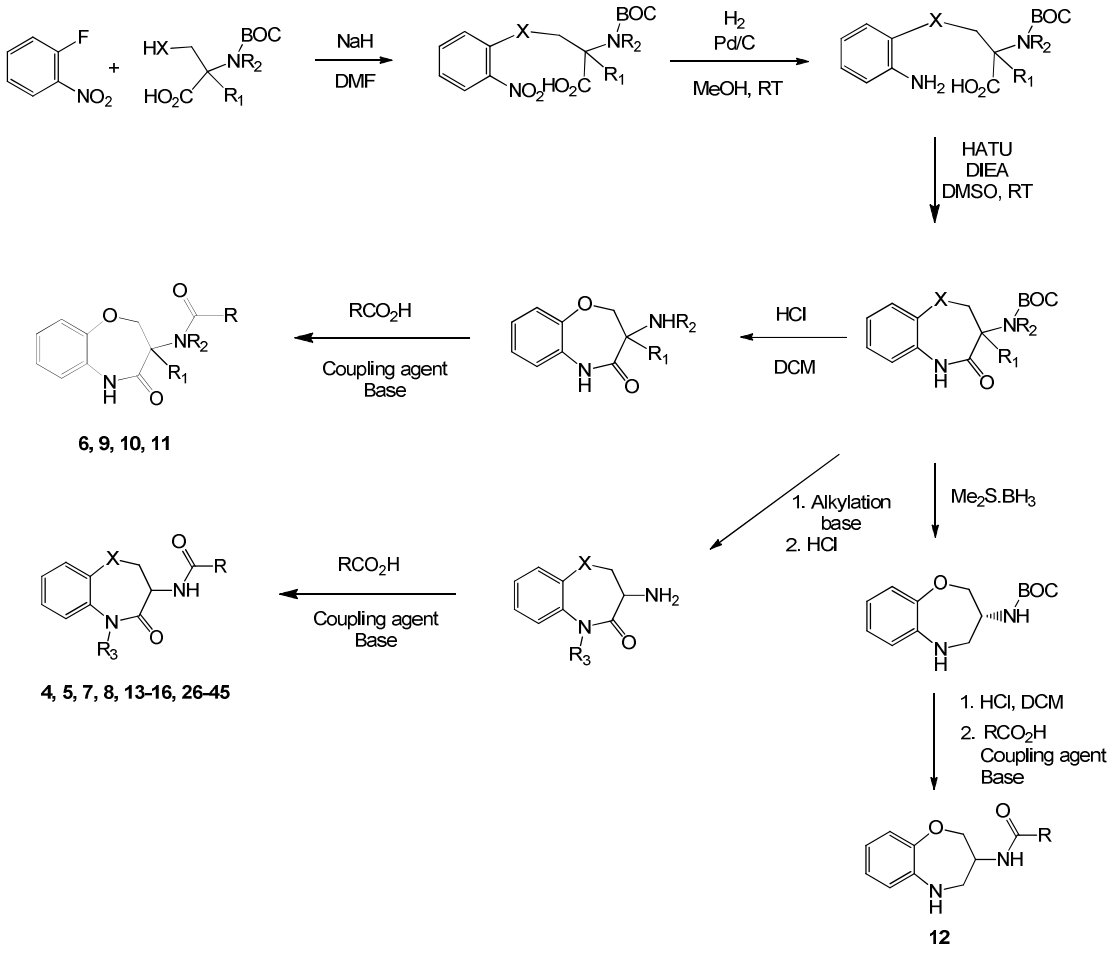

For modifications of the benzoxazepinone heterocycle, the benzo[1,4]oxazocinone **17** was obtained from L-homoserine using similar chemistry, as shown in Scheme 2. The quinolinone **18** was prepared from commercially available 3-amino-3,4-dihydro-2-quinolinone. 1,4-Oxazepan-5-one **19** was obtained starting from coupling of tert-butyl (2-hydroxyethyl)carbamate with *(S)*-1-benzyl 2-methyl aziridine-1,2-dicarboxylate followed by double deprotection. This was

cyclized to Cbz-protected 6-amino-1,4-oxazepan-5-one, which was deprotected and coupled with 5-benzylisoxazole-3-carboxylic acid. The synthesis of the octahydrobenzo[b][1,4]oxazepin-4-one **20** started from *(1R,2R)*-2-aminocyclohexanol. The amine was protected as the *o*-nitrophenylsulfonamide (oNBS) and the alcohol converted to the mesylate. Treatment with base led to conversion to the 7-azabicyclo[4.1.0]heptane, which was ring opened with BOC-L-serine, and on deprotection of the amine this was subsequently cyclized to BOC protected *(3S)*-3-aminooctahydrobenzo[b][1,4]oxazepin-4-one as a 3:1 mixture of trans diastereoisomers. The major diastereoisomer was isolated at this stage, the absolute configuration of the chiral center established by NOE correlations relative to the α proton of (S)-serine, and subsequent deprotection and coupling with 5-benzylisoxazole-3-carboxylic acid yielded **20.**

Scheme 2.

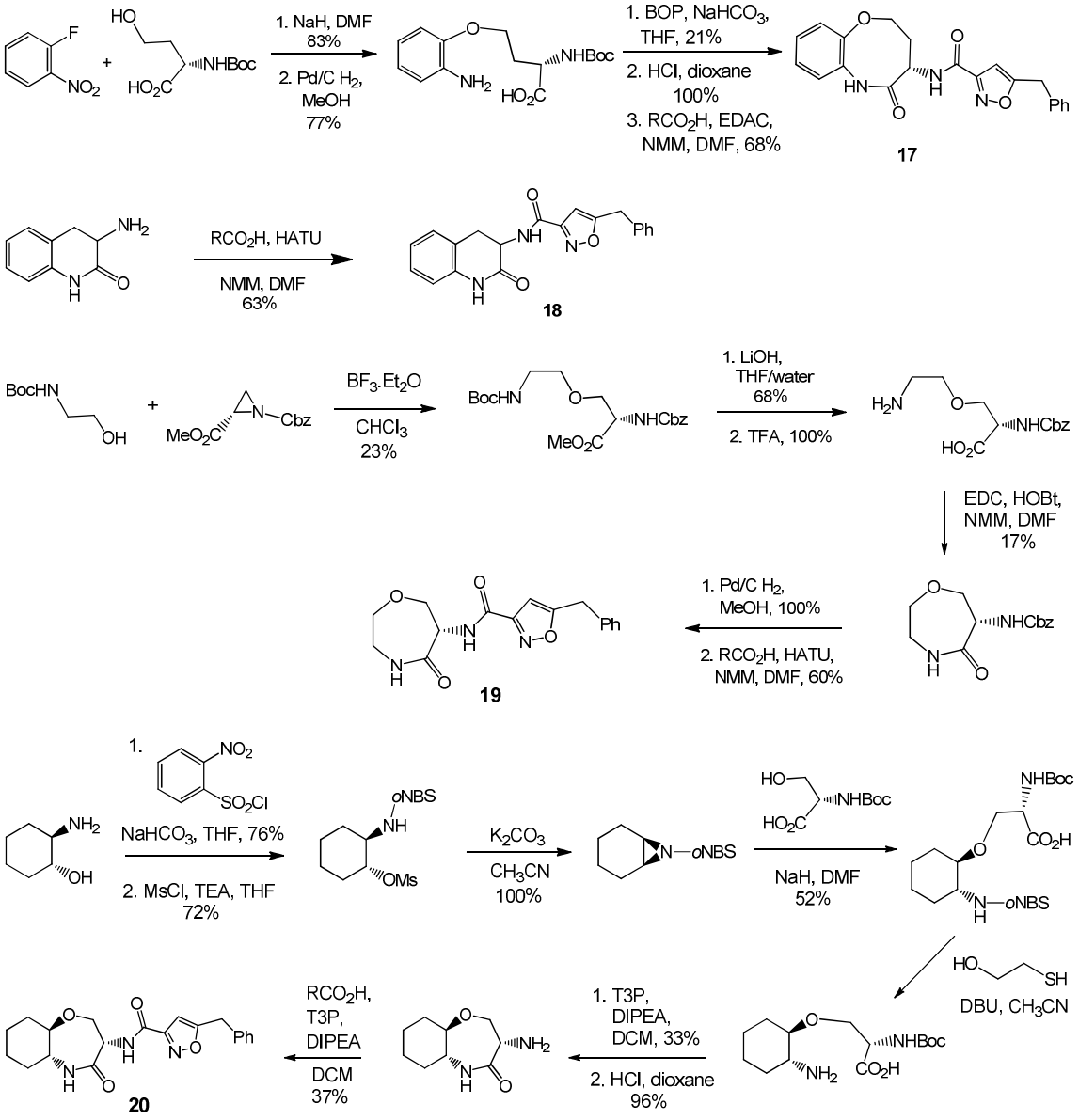

For substitutions at the 7-position of the benzoxazepinone heterocycle, the 7-methyl ester was initially installed following the same benzoxazepinone route outlined earlier, as shown in Scheme 3. The methyl ester was then hydrolyzed and the carboxylic acid converted to the acyl azide by reaction with diphenylphosphoryl azide (DPPA). This underwent Curtius rearrangement to the carbamate in the presence of *tert*-butanol, which was subsequently deprotected to yield the 7-amine. Reaction with acetyl chloride, methyl chloroformate or mesyl chloride gave the analogs **21-23**. To obtain the 7-pyrazole, the 7-bromo benzoxazepinone was prepared using similar

chemistry described earlier, with a nitro reduction using zinc in acetic acid replacing the hydrogenation step. The pyrazole was then installed via a Suzuki coupling with the 3-pyrazoleboronic acid. Finally, the 1,3,4- oxadiazol-2-one (**25**) was obtained from the 7-methyl ester prepared earlier, via ester hydrolysis followed by reaction with hydrazine and carbonyldiimidazole (CDI).

Scheme 3.

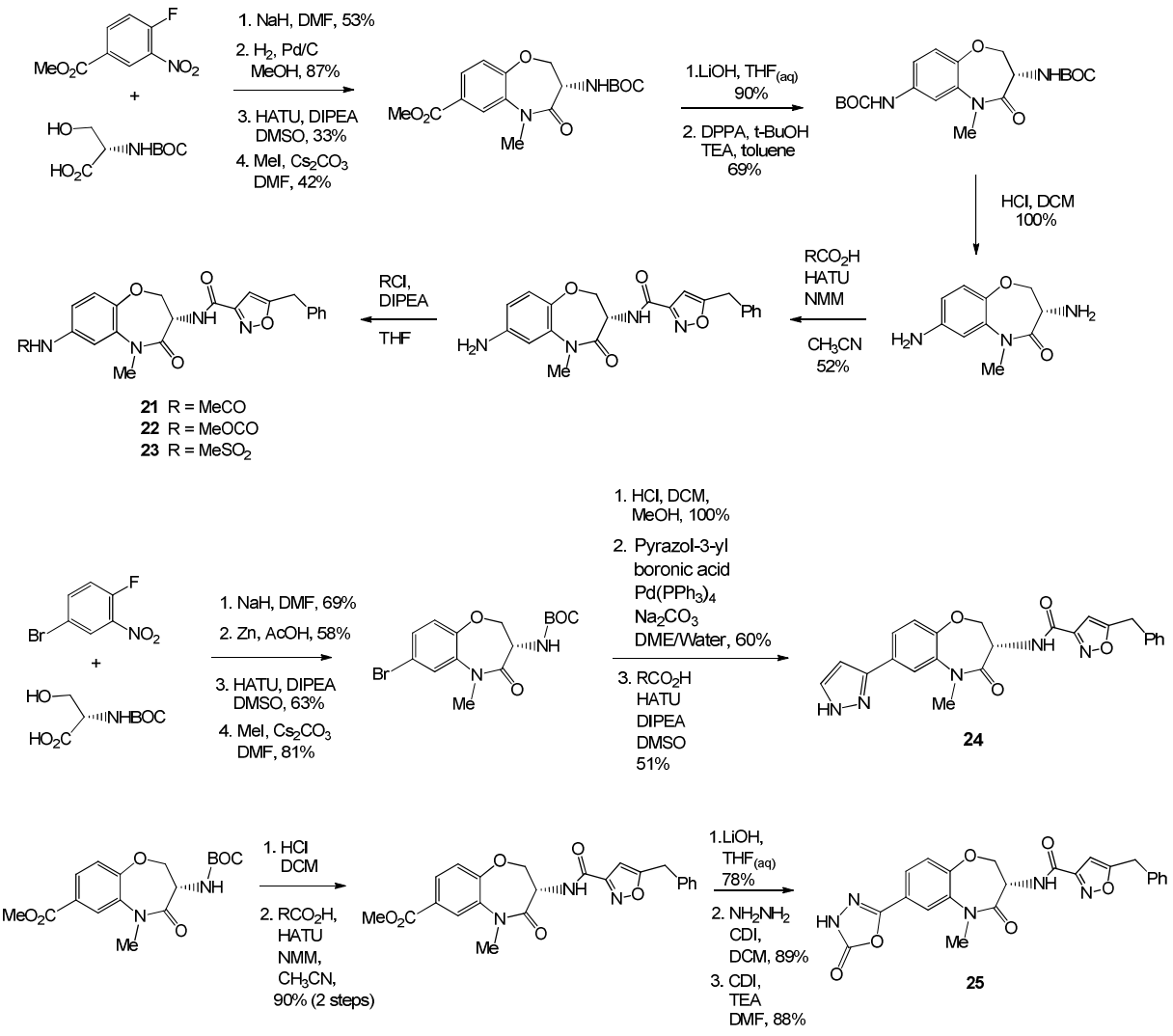

SUMMARY

The emerging biological understanding of the role of RIP1 kinase in regulating necroptosis has opened up an exciting opportunity to explore this as a target for drug intervention in inflammatory disease in the clinic. We identified a novel kinase inhibitor chemotype from a DNA-encoded library with high in vitro RIP1 potency and kinase selectivity. The lead optimization focused on improving the pharmacokinetic and developability profile of the series. Our SAR studies revealed that replacement of the isoxazole of **4** with a triazole was key to improving solubility, lipophilicity and rat oral exposure, leading to the identification of the RIP1 clinical candidate **5**. Benzoxazepinone **5** has excellent activity in both RIP1 cellular systems, preventing TNF induced necrotic cell death, and an ulcerative colitis explant assay blocking spontaneous cytokine release. The compound has highly favorable physicochemical and pharmacokinetic properties, which combined with high potency lead to a predicted once daily low dose in humans. Benzoxazepinone **5** was advanced into phase 1 clinical trials in 2015, and phase 2a clinical trials in psoriasis, rheumatoid arthritis and ulcerative colitis patients are currently underway.

EXPERIMENTAL

General Methods. Unless otherwise noted, starting materials and reagents were purchased from commercial sources and used without further purification. Air or moisture sensitive reactions were carried out under a nitrogen atmosphere. Anhydrous solvents were obtained from Sigma-Aldrich. Microwave irradiation was carried out in a Personal Chemistry Emrys Optimizer microwave. Silica gel chromatography was performed using under standard techniques or using silica gel cartridges (RediSep normal phase disposable flash columns) on an Isco CombiFlash. Reverse phase HPLC purification was conducted on a Gilson HPLC (monitoring at a wavelength of 214 or 254 nm) with a YMC ODS-A C18 column (5 μm, 75 mm 30 mm), eluting with 5-90%

CH_3CN in H_20 with 0.1% TFA unless otherwise noted. ^1H NMR spectra were recorded on a Bruker Advance or Varian Unity 400 MHz spectrometer as solutions in DMSO-d_6 (unless otherwise stated). Chemical shifts (δ) are reported in ppm relative to an internal solvent reference. Apparent peak multiplicities are described as s (singlet), br s (broad singlet), d (doublet), dd (doublet of doublets), t (triplet), q (quartet), or m (multiplet). Coupling constants (J) are reported in hertz (Hz) after the integration.

Sciex LCMS analysis was performed on a PE Sciex Single Quadrupole 150EX, using a Thermo Hypersil Gold (C18, 20 x 2.1 mm, 1.9 u particle diam.), 4-95% CH_3CN:H_2O (with 0.02% TFA) over 2 min., flow rate = 1.4 mL/min. at 55 °C. Waters LCMS was performed using the same column and conditions as for Sciex except using a Waters Acquity SQD UPLC/MS system. The retention time (Rt) is expressed in minutes at a UV detection of 214 or 254 nm. All tested compounds were determined to be ≥95% purity by LCMS (see Supporting Information).

The following compounds were prepared as described previously: *(S)*-5-benzyl-*N*-(5-methyl-4-oxo-2,3,4,5-tetrahydrobenzo[b]-[1,4]oxazepin-3-yl)isoxazole-3-carboxamide (**4**), *(S)*-5-benzyl-*N*-(4-oxo-2,3,4,5-tetrahydrobenzo[b][1,4]-oxazepin-3-yl)isoxazole-3-carboxamide (**6**), *(R)*-5-benzyl-*N*-(4-oxo-2,3,4,5-tetrahydrobenzo[b][1,4]-oxazepin-3-yl)isoxazole-3-carboxamide (**9**), *(R)*-5-benzyl-*N*-(5-methyl-4-oxo-2,3,4,5-tetrahydrobenzo[b]-[1,4]thiazepin-3-yl)isoxazole-3-carboxamide (**13**), *(S)*-5-benzyl-*N*-(1-methyl-2-oxo-2,3,4,5-tetrahydro-1Hbenzo[b]azepin-3-yl)isoxazole-3-carboxamide (**14**), and *(S)*-5-benzyl-*N*-(1-methyl-2-oxo-2,3,4,5-tetrahydro-1Hbenzo[b][1,4]diazepin-3-yl)isoxazole-3-carboxamide (**15**).[22] The following intermediates were prepared as described previously: *(S)*-tert-butyl (4-oxo-2,3,4,5-tetrahydrobenzo[b][1,4]oxazepin-3-yl)carbamate, *(S)*-tert-butyl (2-oxo-2,3,4,5-tetrahydro-1H-

benzo[b][1,4]diazepin-3-yl)carbamate, *(R)*-3-amino-2,3-dihydrobenzo[b][1,4]oxazepin-4(5H)-one.[22]

***(S)*-5-Benzyl-*N*-(5-methyl-4-oxo-2,3,4,5-tetrahydrobenzo[b][1,4]oxazepin-3-yl)-4H-1,2,4-triazole-3-carboxamide (5).** A solution of N-BOC-L-serine (1.0 g, 4.87 mmol) in DMF (2 mL) was added dropwise over 5 min to a suspension of sodium hydride (4.09 g, 10.23 mmol) in DMF (8 mL). Vigorous gas evolution was observed. Once gas evolution had ceased, 1-fluoro-2-nitrobenzene (0.51 mL, 4.87 mmol) was added dropwise neat. The reaction mixture was allowed to stir at rt for 3 h. The reaction mixture was partitioned between ethyl acetate (40 mL) and 0.5 M HCl solution (40 mL). The layers were separated, the organic layer was washed with water (3 x 20 mL), brine (20 mL), and concentrated under reduced pressure to provide the crude product. Purification of the crude material by silica gel chromatography (25-55% EtOAc in hexane) afforded *(S)*-2-((tert-butoxycarbonyl)amino)-3-(2-nitrophenoxy)propanoic acid (1.23 g, 3.77 mmol, 77% yield) as a reddish yellow semi-solid. ^{1}H NMR (400 MHz, $CDCl_3$) δ ppm 7.88 (dd, *J* = 8.46, 1.64 Hz, 1 H), 7.52 - 7.61 (m, 1 H), 7.06 - 7.15 (m, 2 H), 5.68 (br. d., 1 H), 4.75 (br. s., 1 H), 4.60 - 4.72 (m, 1 H), 2.07 (s, 2 H), 1.48 (s, 9 H). Sciex LCMS (m/z) 327 ($M+H^+$), 653 ($2M+H^+$), Rt 0.88 min.

A suspension of *(S)*-2-((tert-butoxycarbonyl)amino)-3-(2-nitrophenoxy)propanoic acid (1.1 g, 3.4 mmol) and palladium on carbon (0.11 g) was exposed to an atmosphere of hydrogen (balloon) overnight (~20 h). Analysis of the crude reaction by LCMS confirmed the formation of the desired product. The slurry was filtered through a 0.45 micron PTFE autovial and the filtrate concentrated under reduced pressure to give *(S)*-3-(2-aminophenoxy)-2-((tert-butoxycarbonyl)amino)propanoic acid (0.98 g, 3.3 mmol, 98% yield) as a pale brown semi solid. The residue was used in the next step without further purification. ^{1}H NMR (DMSO-d_6) δ: 7.42

(br. s., 1H), 6.74 (d, *J* = 7.1 Hz, 1H), 6.64 - 6.70 (m, 1H), 6.57 - 6.62 (m, 1H), 6.47 (td, *J* = 7.6, 1.6 Hz, 1H), 4.40 (d, *J* = 4.3 Hz, 1H), 4.24 (dd, *J* = 9.5, 4.9 Hz, 1H), 4.00 (dd, *J* = 9.6, 3.5 Hz, 1H), 1.41 (s, 9H). Sciex LCMS (m/z) 297 ($M+H^+$), 593 ($2M+H^+$), Rt 0.65 min.

HATU (1.245 g, 3.27 mmol) was added portion wise over 2 min to a solution of *(S)*-3-(2-aminophenoxy)-2-((tert-butoxycarbonyl)amino)propanoic acid (0.97 g, 3.27 mmol) and DIPEA (0.63 mL, 3.6 mmol) in DMSO (12 mL). The reaction mixture was stirred at rt for 30 min. The addition of water (30 mL) resulted in the formation of a precipitate. The mixture was cooled in an ice-bath for 15 min, then was filtered. The collected solid was washed with water and dried in vacuo (high vacuum) to afford *(S)*-tert-butyl (4-oxo-2,3,4,5-tetrahydrobenzo[b][1,4]oxazepin-3-yl)carbamate (0.76 g, 2.73 mmol, 84% yield) as an off-white solid. TLC: 50% EtOAc in Hexane; Rf: 0.55. ^{1}H NMR (400 MHz, DMSO-*d*6) d ppm 9.92 (s, 1 H), 6.99 - 7.21 (m, 5 H), 4.17 - 4.45 (m, 3 H), 1.36 (s, 9 H). Sciex LCMS (m/z) 279 ($M+H^+$), 556 ($2M^+$), Rt 0.87 min.

Methyl iodide (8.09 mL, 129 mmol) was added dropwise during 15 min to a solution of *(S)*-tert-butyl (4-oxo-2,3,4,5-tetrahydrobenzo[b][1,4]oxazepin-3-yl)carbamate (30 g, 108 mmol) and Cs_2CO_3 (49.2 g, 151 mmol) in DMF (300 mL) stirred under nitrogen at room temp. The reaction mixture was stirred at rt for 16 h. TLC (30% EtOAc in Hexane; Rf: 0.4) showed that the reaction was complete. The reaction was poured into cold water (1500 mL) which formed a solid, the resultant solid was filtered, the filter cake was washed with water (two times) and dried in vacuo to afford the crude compound. This was triturated with 5% Et_2O in hexane (300 mL) to afford *(S)*-tert-butyl-(5-methyl-4-oxo-2,3,4,5-tetrahydrobenzo[b][1,4]oxazepin-3-yl)carbamate (19g, 62.7 mmol, 58% yield) as a brown solid. ^{1}H NMR (DMSO-d_6) δ: 7.47 (dd, *J* = 7.7, 1.6 Hz, 1H), 7.23 - 7.33 (m, 2H), 7.14 - 7.21 (m, 2H), 4.25 - 4.41 (m, 3H), 3.28 (s, 3H), 1.34 (s, 9H). Waters LCMS (m/z): 193 (M-BOC), 315 ($M+Na^+$), Rt 0.81 min., >99% purity.

4M HCl (71.8 mL, 287 mmol) was added to a solution of *(S)*-tert-butyl (5-methyl-4-oxo-2,3,4,5-tetrahydrobenzo[b][1,4]oxazepin-3-yl)carbamate (28 g, 96 mmol)) in DCM (300 mL) and the reaction stirred under nitrogen at room temp for 3 h. The solvents were evaporated to dryness to yield the crude compound which was triturated with Et_2O (200 mL), filtered and dried in vacuo to afford *(S)*-3-amino-5-methyl-2,3-dihydrobenzo[b][1,4]oxazepin-4(5H)-one hydrochloride (22.2 g, 97 mmol, >99% yield) as a brown solid. Waters LCMS (m/z): 193 ($M+H^+$), Rt 0.25 min., >99% purity.

T_3P (13.9 mL, 23.4 mmol) and DIPEA (9.5 mL, 54.6 mmol) was added to a stirred solution of *(S)*-3-amino-5-methyl-2,3-dihydrobenzo[b][1,4]oxazepin-4(5H)-one (3.0 g, 15.6 mmol) and 5-benzyl-4H-1,2,4-triazole-3-carboxylic acid (3.49 g, 17.2 mmol) at 0 °C in DCM (100 mL). The reaction mixture was stirred for 30 min at rt and quenched with water (100 mL), the separated DCM phase was washed with 0.1N HCl (50 mL) and brine (50 mL). The DCM phase was dried over Na_2SO_4 and concentrated and the crude product purified by silica gel chromatography (20-70% EtOAc in hexane) to give the title compound (4.7 g, 80 % yield). Recrystallization from EtOAc afforded white crystalline product as the EtOAc solvate. Heating in water at 100 °C for 40 min. and allowing to cool and crystallize removed most of the EtOAc solvate. ^{1}H NMR (DMSO-*d*6) δ ppm 14.41 (br s, 1 H), 8.48 (br s, 1 H), 7.50 (dd, *J* = 7.7, 1.9 Hz, 1 H), 7.12-7.40 (m, 8 H), 4.83 (dt, *J* = 11.6, 7.9 Hz, 1 H), 4.60 (t, *J* = 10.7 Hz, 1 H), 4.41 (dd, *J* = 9.9, 7.8 Hz, 1 H), 4.12 (s, 2 H), 3.31 (s, 3 H). Anal. Calcd for $C_{20}H_{20}N_5O_3 \cdot 0.026EtOAc \cdot 0.4H_2O$ C, 62.36; H, 5.17; N, 18.09. Found: C, 62.12; H, 5.05; N, 18.04.

Fluorescence Polarization (FP) Binding Assay. A fluorescent polarization based binding assay was utilized using competition with a fluorescently labeled ATP competitive ligand (14-(2-{[3-({2-{[4-(cyanomethyl)phenyl]amino}-6-[(5-cyclopropyl-1H-pyrazol-3-yl)amino]-4-

pyrimidinyl}amino)propyl]amino}-2-oxoethyl)-16,16,18,18-tetramethyl-6,7,7a,8a,9,10,16,18-octahydrobenzo[2",3"]indolizino[8",7":5',6']pyrano[3',2':3,4]pyrido[1,2-a]indol-5-ium-2-sulfonate. The assay was conducted as previously described and in the Supporting Information with at least n = 2 and the mean IC_{50} reported.[22]

ADP-Glo Activity Assay. The catalytic activity of RIP1 was quantified utilizing the Promega ADP-Glo kinase kit as previously described and in the Supporting Information using either a four parameter curve fit or a tight binding curve fit for compounds whose potency was less than the detection limit of the assay (~ half the enzyme concentration).[22] Data are presented as the mean IC_{50} from at least n=2 determinations.

U937and L929 Cell Necroptosis Assay. The efficacy of RIP1 inhibitors were determined in vitro using human monocytic leukemia U937 cells or mouse L-cells NCTC 929 (L929) cells in a necroptosis assay as previously described.[22]

Biological in Vitro Whole Blood Assay. Compound **5** was evaluated in human and cynomolgus monkey whole blood assays. For the assay, 3 stock solutions each of 200 ng/mL TNF (Cell Sciences), 400 μM QVD-OPh or zVAD.fmk (R&D Systems) and 20 μM 2',2'''-(2,4-hexadiyne-1,6-diyl)bis[1-[[(2S)-1-(*N*-methyl-L-alanyl-L-threonyl)-2-pyrrolidinyl]methyl]-5-(phenylthio)-1H-tetrazole (RMT 5265[29]) were prepared in phenol red free RPMI 1640 medium supplemented with 1% fetal bovine serum, 100 units/mL penicillin and 100 μg/mL streptomycin. In addition 5-fold dilution series of compound **5** were prepared in the same medium supplemented with 1% DMSO, with top concentrations of 1 μM and 5 μM for human and monkey assays, respectively. A 5 uL solution of compound **5** at each dilution was transferred to a 96 well tissue culture treated assay plate and 5 uL of each of the 3 stock solutions was added. Whole blood was collected by venous puncture in heparin tubes (Griener Bio-One). Whole blood

(80 μL) was added to each well of the assay plate, mixed briefly and incubated for 6 h at 37 ^{o}C, 5% CO_2. Following incubation, PBS (200 μL) was added to each well and the assay plate was centrifuged at 1700 rpm for 5 min. Supernatants were frozen at -70^{o} C. Concentrations of MIP-1β (human) and IL-1β (monkey) were determined by sandwich ELISA (Meso Scale Discovery) following the manufacturer's instructions.

Neutrophil Necroptotic Assay.

Compound **5** was evaluated in human neutrophils isolated from whole blood using standard method involving dextran sedimentation and Ficoll-Hypaque density gradient centrifugation. Necroptotic cell death was induced in freshly isolated neutrophils with 10 ng/ml TNFα, 50μM QVD-OPh and 100 nM SMAC mimetic 2',2'''-(2,4-hexadiyne-1,6-diyl)bis[1-[[(2S)-1-(N-methyl-L-alanyl-L-threonyl)-2-pyrrolidinyl]methyl]-5-(phenylthio)-1H-tetrazole (SMAC mimetic RMT 5265[29]). Induced cell death was evaluated 21 h post stimulation by measuring cellular ATP levels and LDH release into media. Intracellular ATP levels were quantified using CellTiter-Glo Luminescent Cell Viability assay (Promega). Lactate dehydrogenase (LDH) release into media was evaluated using a Cytotoxicity Detection kit [LDH] (Roche Applied Sciences). Concentration of MIP-1β in cell-free supernatants was determined by sandwich ELISA (Meso Scale Discovery) following the manufacturer's instructions.

Organ Culture of Human Intestine Mucosal Explants. Tissue was obtained during routine endoscopy of patients with IBD. All patients took part in this study after providing informed written consent. The study was approved by the local ethics committee. Explant cultures were performed as previously described.[30] Biopsies were cultured in 24-well plates in 300 μL of serum-free HL1 medium (Lonza, Cambridge, England) containing glutamine, Pen/Strep, and 50 mg/mL gentamicin. The RIP1 kinase inhibitor was added to the culture medium. Mucosal

samples were immersed in liquid, and culture was performed for 24 h at 37 °C and 5% CO_2. Supernatants and biopsies were subsequently snap-frozen and stored at −70 °C. Cytokine concentrations of IL-1β and IL-6 were determined by Sandwich ELISA (R&D Systems) according to the manufacturer's instructions. The human biological samples were sourced ethically and their research use was in accord with the terms of the informed consents.

Biological in Vivo Assay. The efficacy of RIP1 inhibitors can be tested in mice in vivo using a TNF-driven systemic inflammatory response syndrome model.[31] A total of 7 mice per dose group were orally pre-dosed with saline or compound **5** at doses of 3, 10 and 50 mg/kg 15 min before iv administration of mouse TNF (30 μg/mouse). Temperature loss in the mice was measured by rectal probe. The study was terminated after 6 hours when the control group lost 7 °C. In a similar model, injection of TNF combined with the caspase inhibitor zVAD leads to a similar but earlier onset systemic inflammatory response in about 3 hours. A total of 7 mice per dose group were orally pre-dosed with vehicle (saline + zVAD at 0.4 mg/mouse) or compound **5** at doses of 3, 10 and 50 mg/kg 15 min, before iv administration of mouse TNF (30 μg/mouse) and zVAD (0.4 mg/mouse). The study was terminated after 3 hours when the control group lost 7 °C. All data are shown as means ± standard error of the mean.

Human biological samples were sourced ethically and their research use was in accord with the terms of the informed consents. All studies involving the use of animals were conducted after review by the GlaxoSmithKline (GSK) Institutional Animal Care and Use Committee and in accordance with the GSK Policy on the Care, Welfare and Treatment of Laboratory Animals.

ASSOCIATED CONTENT

Supporting Information

Supporting Information. Preparation of compounds **7**, **8**, **10-12**, **16-45**, enzyme preparations, mode of inhibition of hRIP1 activity in the ADP-GLO activity assay, CHI log *D* and kinetic aqueous solubility measurements for compounds **4-45**. Enzyme kinetics, kinase selectivity profile, RIP1 co-crystallization, rat tissue distribution, permeability and P-gp substrate evaluation, microsomal and hepataocyte turnover for compound **5**.

Accession Codes

Coordinates and structure factors for the cocrystal structure of RIP1 (1−294, C34A, C127A, C233A, C240A) and benzoxazepinone **5** have been deposited in the Protein Data Bank with the accession number 5TX5.

AUTHOR INFORMATION

Corresponding Author

* E-mail: philip.a.harris@gsk.com.

Author Contributions

John Bertin and Peter J. Gough contributed equally to this work. All authors have given approval to the final version of the manuscript.

Notes

The authors declare the following competing financial interests: All authors, with the exception of Thomas T. MacDonald, Anna Vossenkämper and Barbara A. Swift, are current employees and stockholders of GlaxoSmithKline.

ABBREVIATIONS USED

ADMET, absorption, distribution, metabolism, excretion, and toxicity; BOC, tert-butyloxycarbonyl; CDI, carbonyldiimidazole; CYP, cytochrome P450; DFG, Asp-Phe-Gly; DIPEA, diisopropylethylamine; DMAP, 4-dimethylaminopyridine; EDAC, 1-ethyl-3-(3-dimethylaminopropyl)carbodiimide; FasL, Fas ligand; FaSSIF, fasted state simulated intestinal fluid; FP, fluorescence polarization; HATU, 1-[bis(dimethylamino)methylene]-1H-1,2,3-triazolo[4,5-b]pyridinium 3-oxide hexafluorophosphate; HEK, human embryonic kidney; hERG, human ether-a-go-go-related gene; HOBT, hydroxybenzotriazole; hPXR, human pregnane X receptor; LDH, lactate dehydrogenase; MIP, macrophage inflammatory protein; RIP1, receptor interacting protein 1; PTFE, polytetrafluoroethylene; QVD-OPh, (3S)-5-(2,6-difluorophenoxy)-3-[[(2S)-3-methyl-1-oxo-2-[(2-quinolinylcarbonyl)amino]butyl]amino]-4-oxopentanoic acid hydrate; SMAC, second mitochondrial-derived activator of caspases; T_3P, 2,4,6-tripropyl-1,3,5,2,4,6-trioxatriphosphinane 2,4,6-trioxide; TEA, triethylamine; TNF, tumor necrosis factor; TNFR1, tumor necrosis factor receptor 1; TRAIL, TNF-related apoptosis-inducing ligand; zVAD.fmk, carbobenzoxy-valyl-alanyl-aspartyl-[O-methyl]- fluoromethylketone.

REFERENCES

1. Berger, S. B.; Kasparcova, V.; Hoffman, S.; Swift, B.; Dare, L.; Schaeffer, M.; Capriotti, C.; Cookm M.; Finger, J.; Hughes-Earle, A.; Harris, P. A.; Kaiser, W. J.; Mocarski E. S.; Bertin, J.; Gough, P. J. Cutting Edge: RIP1 Kinase Activity is Dispensable for Normal Development but is a Key Regulator of Inflammation in SHARPIN-Deficient Mice. *J. Immunol.* **2014**, *192*, 5476-5480.

2. Takahashi, N.; Vereecke, L.; Bertrand, M. J. M.; Duprez, L.; Berger, S. B.; Divert, T.; Goncalves, A.; Sze, M.; Gilbert, B.; Kourula, S.; Goossens, V.; Lefebvre, S.; Gunther, C.; Becker, C.; Bertin, J.; Gough, P. J.; Declercq, W.; van Loo, G.; Vandenabeele, P. RIPK1 Ensures Intestinal Homeostasis by Protecting the Epithelium Against Apoptosis. *Nature* **2014** *513*, 95-99.

3. Dannappel, M.; Vlantis, K.; Kumari, S.; Polykratis, A.; Kim, C.; Wachsmuth, L.; Eftychi, C.; Lin, J.; Corona, T.; Hermance, N.; Zelic, M.; Kirsch, P.; Basic, M.; Bleich, A.; Kelliher, M.; Pasparakis M. RIPK1 Maintains Epithelial Homeostasis by Inhibiting Apoptosis and Necroptosis. *Nature* **2014** *513*, 90-94.

4. Gunther, C.; Martini, E.; Wittkopf, N.; Amann, K.; Weigmann, B.; Neumann, H.; Waldner, M. J.; Hedrick, S. M.; Tenzer, S.; Neurath, M. F.; Becker, C. Caspase-8 Regulates TNF-alpha-induced Epithelial Necroptosis and Terminal Ileitis. *Nature* **2011**, *477*, 335-339.

5. Bonnet, M. C.; Preukschat, D.; Welz, P. S.; van Loo, G.; Ermolaeva, M. A.; Bloch, W.; Haase, I.; Pasparakis, M. The Adaptor Protein FADD Protects Epidermal Keratinocytes From Necroptosis In Vivo and Prevents Skin Inflammation. *Immunity* **2011**, *35*, 572-582.

6. Welz, P. S.; Wullaert, A.; Vlantis, K.; Kondylis, V.; Fernandez-Majada, V.; Ermolaeva, M.; Kirsch, P.; Sterner-Kock, A.; van Loo, G.; Pasparakis, M. FADD Prevents RIP3-Mediated Epithelial Cell Necrosis and Chronic Intestinal Inflammation. *Nature* **2011**, *477*, 330-334.

7. Christofferson, D. E.; Yuan, J. Necroptosis as an Alternative Form of Programmed Cell Death. Curr. Opin. *Cell Biol*. **2010**, *22*, 263-268.

8. Galluzzi, L.; Kroemer, G. Necroptosis: a Specialized Pathway of Programmed Necrosis. *Cell* **2008**, *135*, 1161-1163.

9. Christofferson, D. E.; Li, Y.; Hitomi, J.; Zhou, W.; Upperman, C.; Zhu, H.; Gerber, S. A.; Gygi, S.; Yuan, J. A Novel Role For RIP1 kinase in Mediating TNF[alpha] Production. *Cell Death Dis*. **2012**, e320.

10. Duong, B. H.; Onizawa, M.; Oses-Prieto, J. A.; Advincula, R.; Burlingame, A.; Malynn, B. A.; Ma, A. A20 Restricts Ubiquitination of Pro-Interleukin-1beta Protein Complexes and Suppresses NLRP3 Inflammasome Activity. *Immunity* **2015**, *42*, 55-67.

11. Jouan-Lanhouet, S.; Arshad, M. I.; Piquet-Pellorce, C.; Martin-Chouly, C.; Le Moigne-Muller, G.; Van Herreweghe, F.; Takahashi, N.; Sergent, O.; Lagadic-Gossmann, D.; Vandenabeele, P.; Samson, M.; Dimanche-Boitrel, M. T. TRAIL Induces Necroptosis Involving RIPK1/RIPK3-Dependent PARP-1 Activation. *Cell Death Differ.* **2012**, *19*, 2003-2014.

12. Najjar, M.; Saleh, D.; Zelic, M.; Nogusa, S.; Shah, S.; Tai, A.; Finger, J. N.; Polykratis, A.; Gough, P. J.; Bertin, J.; Whalen, M. J.; Pasparakis, M.; Balachandran, S.; Kelliher, M.; Poltorak, A.; Degterev, A. RIPK1 and RIPK3 kinases Promote Cell-Death Independent Inflammation by Toll-Like Receptor 4. *Immunity* **2016**, *45*, 46-59.

13. McNeal, S. I.; LeGolvan, M. P.; Chung, C. S.; Ayala, A.The Dual Functions of RIP1 in FAS-induced Hepatocyte Death During Sepsis. *Shock* **2011**, *35*, 499-505.

14. Degterev, A.; Hitomi, J.; Germscheid, M.; Ch'en, I. L.; Korkina, O.; Teng, X.; Abbott, D.; Cuny, G. D.; Yuan, C.; Wagner, G.; Hedrick, S. M.; Gerber, S. A.; Lugovskoy, A.; Yuan,

J. Identification of RIP1 Kinase as a Specific Cellular Target of Necrostatins. *Nat. Chem. Biol*. **2008**, *4*, 313-321.

15. Degterev, A.; Huang, Z.; Boyce, M.; Li, Y.; Jagtap, P.; Mizushima, N.; Cuny, G. D.; Mitchison, T. J.; Moskowitz M. A.; Yuan J. Chemical Inhibitor of Nonapoptotic Cell Death With Therapeutic Potential for Ischemic Brain Injury. *Nat. Chem. Biol*. **2005**, *1*, 112-119.

16. Xie, T.; Peng, W.; Liu, Y.; Yan, C.; Maki, J.; Degterev, A.; Yuan, J.; Shi Y. Structural Basis of RIP1 Inhibition by Necrostatins. *Structure* **2013**, *21*, 493-499.

17. Christofferson, D. E; Li, Y.; Hitomi, J.; Zhou, W.; Upperman, C.; Zhu, H.; Gerber, S. A.; Gygi, S.; Yuan J. A Novel Role for RIP1 Kinase in Mediating TNFα Production. *Cell Death Dis*. **2012**, 3,e320.

18. Teng, X.; Degterev, A.; Jagtap, P.; Xing, X.; Choi, S.; Denu, R.; Yuan, J.; Cuny, G. D. Structure-activity Relationship Study of Novel Necroptosis Inhibitors. *Bioorg Med Chem Lett.* **2005**, *15*, 5039-5044.

19. Harris, P. A.; Bandyopadhyay, D.; Berger, S. B.; Campobasso, N.; Capriotti, C. A.; Cox, J. A.; Dare, L.; Finger, J. N.; Hoffman, S. J.; Kahler, K. M.; Lehr, R.; Lich, J. D.; Nagilla, R.; Nolte, R. T.; Ouellette, M. T.; Pao, C. S.; Schaeffer, M. C.; Smallwood, A.; Sun, H. H.; Swift, B. A.; Totoritis, R. D.; Ward, P.; Marquis, R. W.; Bertin, J.; Gough, P. J. Discovery of Small Molecule RIP1 Kinase Inhibitors for the Treatment of Pathologies Associated With Necroptosis. *ACS Med Chem Lett*. **2013**, *4*, 1238-1243.

20. Berger, S. B.; Harris, P.; Kasparcova, K.; Hoffman, S.; Swift, B.; Dare, L.; Schaeffer, M.; Capriotti, C.; Ouellette, M.; King, B. W.; Wisnoski, D.; Cox, J.; Relly, M.; Marquis, R. W.; Bertin, J.; Gough, P. J. Characterization of GSK′963: a Structurally Distinct, Potent and Selective Inhibitor of RIP1 Kinase. *Cell Death Disc*. **2015**, *1*, 15009.

21. Clark, M. A.; Acharya, R. A.; Arico-Muendel, C. C.; Belyanskaya, S. L.; Benjamin, D. R.; Carlson, N. R.; Centrella, P. A.; Chiu, C. H.; Creaser, S. P.; Cuozzo, J. W.; Davie, C. P.; Ding, Y.; Franklin, G. J.; Franzen, K. D.; Gefter, M. L.; Hale, S. P.; Hansen, N. J. V.; Israel, D. I.; Jiang, J.; Kavarana, M. J.; Kelley, M. S.; Kollmann, C. S.; Li, F.; Lind, K.; Mataruse, S.; Medeiros, P. F.; Messer, J. A.; Myers, P.; O'Keefe, H.; Oliff, M. C.; Rise, C. E.; Satz, A. L.; Skinner, S. R.; Svendsen, J. L.; Tang, L.; Vloten, K. V.; Wagner, R. W.; Yao, G.; Zhao, B.; Morgan, B. A. Design, Synthesis and Selection of DNA-Encoded Small-molecule Libraries. *Nat. Chem. Biol*. **2009**, *5*, 647−654.

22. Harris, P. A.; King, B. W.; Bandyopadhyay, D.; Berger, S. B.; Campobasso, N.; Capriotti, C. A.; Cox, J. A.; Dare, L.; Dong, X.; Finger, J. N.; Grady, L. C.; Hoffman, S. J.; Jeong, J. U.; Kang, J.; Kasparcova, V.; Lakdawala, A. S.; Lehr, R.; McNulty, D.E.; Nagilla, R.; Ouellette, M. T.; Pao, C. S.; Rendina, A. R.; Schaeffer, M. C.; Summerfield, J. D.; Swift, B.A.; Totoritis, R.D.; Ward, P.; Zhang, A.; Zhang, D.; Marquis, R. W.; Bertin, J.; Gough, P. J. DNA-Encoded Library Screening Identifies Benzo[B][1,4]Oxazepin-4-Ones as Highly Potent and Monoselective Receptor Interacting Protein 1 Kinase Inhibitors. *J. Med. Chem*. **2016**, *59*, 2163-2178.

23. Valkó, K. Chromatographic Hydrophobicity Index by Fast-gradient RP-HPLC: a High-throughput Alternative to Log P/Log D. *Anal. Chem*. **1997**, *69*, 2022–2029.

24. Reid, R. C.; Yau, M. K.; Singh, R.; Lim, J.; Fairlie, D. P. Stereoelectronic Effects Dictate Molecular Conformation and Biological Function of Heterocyclic Amides. *J Am. Chem. Soc.* **2014**, *136*, 11914-11917.

25. Kestranek, A.; Chervenak, A.; Longenberger, J.; Placko, S. Chemiluminescent Nitrogen Detection (CLND) to Measure Kinetic Aqueous Solubility. *Curr Protoc Chem Biol*. **2013**, *5*, 269-280.

26. Ritchie, T. J.; Macdonald, S. J. F.; Peace, S.; Pickett, S. D.; Luscombe, C. N. The Developability of Heteroaromatic and Heteroaliphatic Rings − Do Some Have a Better Pedigree as Potential Drug Molecules Than Others? *MedChemComm* **2012**, *3*, 1062−1069.

27. Katritzky, A. R.; Ramsden, C. A.; Joule, J. A.; Zhdankin, V. V. Struture of Five-membered Rings With Two or More Heterocycles. In *Handbook of Heterocyclic Chemistry*, 3rd ed.; Elsevier: Oxford, 2010; pp 149-150.

28. Müller, S.; Chaikuad, A.; Gray, N. S.; Knapp, S. The Ins and Outs of Selective Kinase Inhibitor Development. *Nat. Chem. Biol.* **2015**, *11*, 818-821.

29. Li, L.; Thomas, R. M.; Suzuki, H.; De Brabander, J. K.;, Wang, X.; Harran, P. G. A Small Molecule Smac Mimic Potentiates TRAIL- and TNFalpha-mediated Cell Death. *Science* **2004**, *305*, 1471-1474.

30. Vossenkämper, A.; Hundsrucker, C.; Page, K.; van Maurik, A.; Sanders, T. J.; Stagg, A. J.; Das, L.; MacDonald, T. T. A CD3-specific Antibody Reduces Cytokine Production and Alters Phosphoprotein Profiles in intestinal Tissues From Patients With Inflammatory Bowel Disease. *Gastroenterology* **2014**, *147*, 172−183.

31. Duprez, L.; Takahashi, N.; Van Hauwermeiren, F.; Vandendriessche, B.; Goossens, V.; Vanden Berghe, T.; Declercq, W.; Libert, C.; Cauwels, A.; Vandenabeele, P. RIP Kinase-Dependent Necrosis Drives Lethal Systemic Inflammatory Response Syndrome. *Immunity* **2011**, *35*, 908−918.

Table of Contents graphic

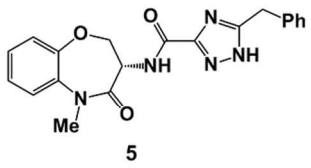

5

RIP1 clinical candidate